PROCEEDINGS, 41st Workshop on Geothermal Reservoir Engineering
Stanford University, Stanford, California, February 22-24, 2016
SGP-TR-209

Geologic Setting of the Idaho National Laboratory Geothermal Resource Research Area

Michael McCurry[1], Travis McLing[2], Richard P. Smith[3], William R. Hackett[4], Ryan Goldsby[1], William Lochridge[1], Robert Podgorney[2], Thomas Wood[5], David Pearson[1], John Welhan[6], Mitch Plummer[2]

[1]Department of Geosciences, Idaho State University, Pocatello, ID 83209

[2]Idaho National Engineering Laboratory, Idaho Falls, ID 83415

[3]Smith Geologic and Photographic Services, LLC, 13786 Schoger Road, Nathrop, CO 81236

[4]WRH Associates, Inc., 2007 Cherokee Circle, Ogden, UT 84403

[5]University of Idaho, Center for Advanced Energy Studies, Idaho Falls, ID 83402

[6]Idaho Geological Survey, University of Idaho, Moscow, ID 83844

e-mail: Michael McCurry <mccumich@isu.edu>

Keywords: Snake River Plain, geologic conceptual model, subsurface geology, rhyolite, caldera, EGS

ABSTRACT

The Idaho National Laboratory (INL) has designated ~100 km^2 of the Eastern Snake River Plain (ESRP), along the track of the Yellowstone Hot Spot, as a Geothermal Resource Research Area (GRRA). The GRRA is a designated area of the INL Site to support research and development for all aspects of geothermal energy. The GRRA is the focus of studies under the Phase I award to the Snake River Geothermal Consortium (SRGC) from the DOE Frontier Observatory Research in Geothermal Energy (FORGE) program. The GRRA provides a robust field site for development of innovative and advanced geothermal technologies, approaches and methods.

The GRRA is located in a geological region that is dominated by the Yellowstone volcanic track, the Earth's largest and most active continental hot spot system. It is well known for high regional heat flow (110 mW/m^2) and voluminous late Miocene to Holocene magmatism and tectonism. The GRRA is generally underlain by several hundred meters of interbedded Pleistocene basalt lavas erupted from widely scattered vents on the ESRP and sediment derived from mountain ranges northwest of the plain. The basalts and sediments host part of the prolific ESRP aquifer. In the adjacent 3.2 km deep INEL-1 well, these rocks overlie thousands of meters of rhyolites erupted during the climax of hot spot related volcanic activity between ~10 and 4.5 Ma. The rhyolites are dominantly voluminous densely welded ignimbrites, lava flows and shallow intrusions that ponded within and intruded beneath and into coeval caldera systems. Permeability of the thick intracaldera deposits is extremely low due to a combination of very dense welding and rock alteration and mineralization driven by now-extinct intracaldera hydrothermal systems. The extremely low permeability and large mass of the hot deep rocks is ideally suited for EGS studies as heat recovery from this region will require advanced drilling, reservoir stimulation, and fluid injection to achieve necessary heat extraction.

1. INTRODUCTION

The Eastern Snake River Plain (ESRP) is one of the largest regions in North America of high heat flow (up to 110 mW/m^2) and robust volcanic and tectonic activity (e.g., Blackwell, 1989; Anders et al., 2014). Recent activity is dominated by Yellowstone-Snake River Plain hot spot system (e.g., Smith et al., 2009). Enormous overlapping and nested calderas were produced by voluminous rhyolitic volcanic eruptions between 10 and 4.6 Ma, producing potentially ideal host-rock materials for development of EGS technologies. However, post-caldera basaltic volcanism, and the development of a robust active aquifer system have muted obvious surficial evidence of the underlying caldera systems and high heat flow (e.g., Smith, 2004). Locations and characteristics of buried (cryptic) calderas are therefore inferred from robust regional geologic and geophysical surveys, and from deep borehole data.

This paper is a preliminary summary of the geologic setting and evolution of the Geothermal Resources Research Area (GRRA), emphasizing materials, structures and cryptic caldera context of the proposed EGS reservoir system. It summarizes and integrates previous work with the focus being to develop a geologically and geophysically constrained range of conceptual models of GRRA subsurface geologic architecture at geothermal-reservoir-relevant depths of 1.5 to 4 km.

2. REGIONAL GEOLOGIC SETTING

The GRRA site is located on the northern margin of the Yellowstone-Snake River Plain (YSRP) volcanic track, the worlds largest active continental hot spot system (e.g., Smith et al. 2009) (Fig. 1).

The crust in this region consists mainly of early Precambrian crystalline rocks (Foster et al., 2006) that are overlain by late Precambrian to Mesozoic age sedimentary rocks of the Cordilleran fold and thrust belt (Dickinson, 2004; DeCelles and Coogan, 2006; Yonkee et al., 2014). Regional magmatic activity produced the late Cretaceous Idaho Batholith and Eocene Challis volcanic province (e.g., Gaschnig et al., 2011) and Oligocene intrusions of the Albion Mountains region (Konstantinou et al., 2012, 2013a). But with the exception of distal sedimentary facies of the Challis system, none of these appear to have extended to the GRRA area (Fig. 2A). Strong extension

occurred in Eocene to early Oligocene exposing mid-crustal rocks in isolated metamorphic core complexes of the Pioneer and Albion-Raft River Mountains areas, northwest and southwest of GRRA (Strickland et al., 2011a,b). Coeval, less intense extension produced half graben basins over a wider region, including formation of the Arco Pass Basin located just north of the GRRA in the Arco Hills (e.g., Link and Janecke, 1999). Another, later phase of late Miocene extension and uplift occurred during proximal volcanism along the YSRP (Vogel et al., 2014; Konstantinou et al.. 2011, 2013b).

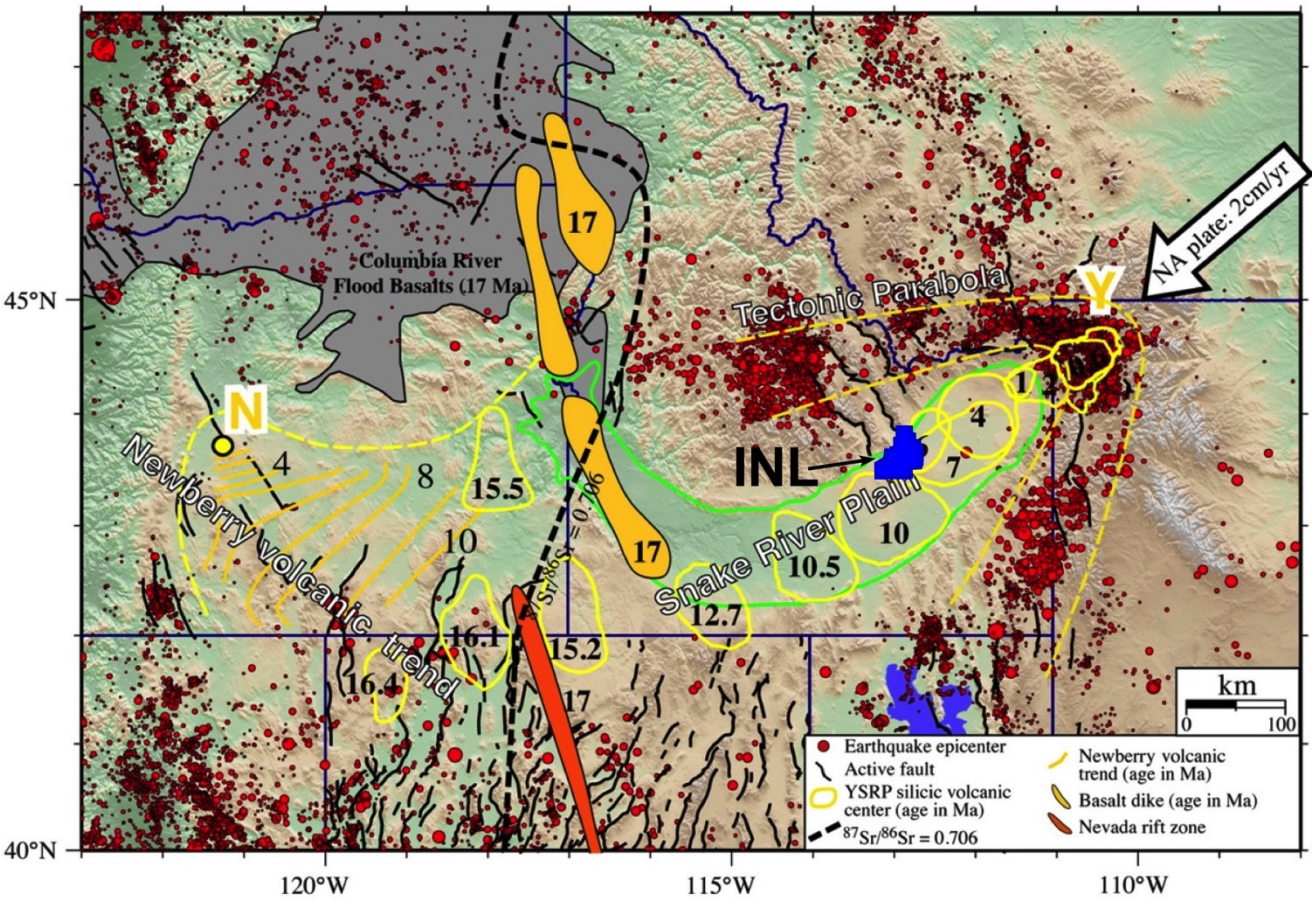

Figure 1: The location and regional geologic and tectonic setting of the proposed GRRA and FORGE Phase 1 study area (after Smith et al., 2009, their figure 2). The GRRA is located on the northwest margin of the INL (shown in dark blue). The map emphasizes major Neogene to Recent volcanic and tectonic features related to development and evolution of the Nevada-Columbia magmatic belt (Camp et al., 2015) and the Yellowstone-Snake River Plain hotspot system. Most lines and symbols are explained on the inset explanation. Ages of initiation of major silicic volcanism are indicated for rhyolite volcanic fields (yellow lines). The green line encompasses Quaternary to Pliocene basalt lavas that postdate local rhyolite volcanism.

Regional Basin-and-Range extension began ~17-15 Ma and is continuing to present, most actively in eastern and western regions of Basin and Range (e.g., Parsons, 1995), and around the margins of the ESRP - the YSRP "tectonic parabola" (e.g., Anders et al., 1989) (Fig. 1). Inception of Basin and Range extension coincided with massive 17-15 Ma outpouring of basalt lavas of the Columbia River Basalt (CRB) Large Igneous Province (LIP) (e.g., Camp et al., 2015) (Fig. 1). Numerous studies suggest that initiation of extension, coeval CRB volcanism, volcanism in southeastern Oregon, and southward across central Nevada are genetically linked to upward impingement of a mantle plume on the base of the North American lithosphere (e.g., Pierce et al., 2009).

Basaltic CRB volcanism is followed by two time-transgressive tracks of rhyolite-dominated volcanism. A weaker northwest trending track, the Oregon High Lava Plains track (Fig. 1, Newberry volcanic trend), and a much more robust track that extends to the northeast across southern Idaho and currently located beneath the Yellowstone, Wyoming region (referred to here as the YSRP track, for Yellowstone-Snake River Plain) (Fig. 1, 2A).

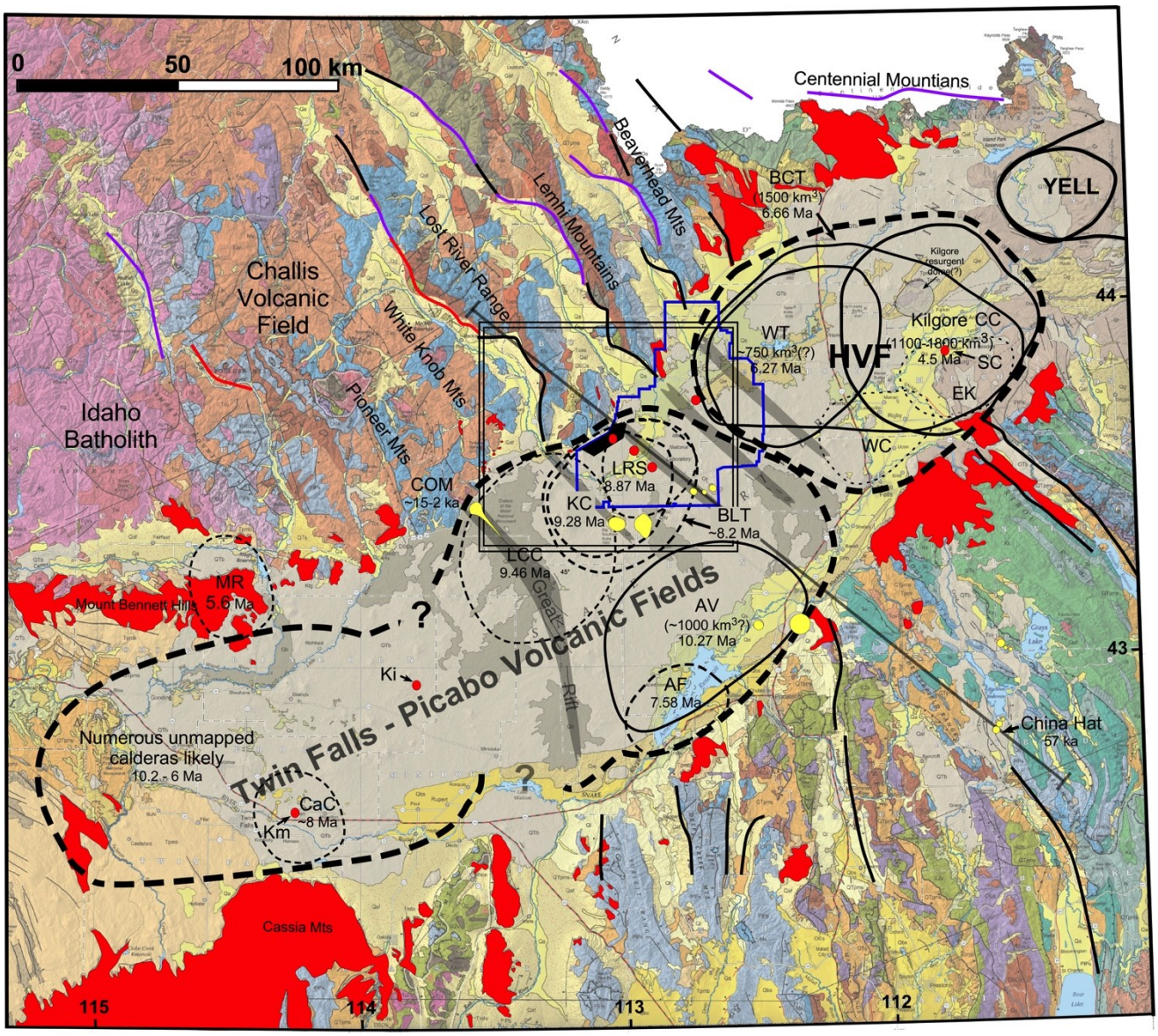

Figure 2. Geologic map of the Eastern Snake River Plain (ESRP) and its surroundings emphasizing salient volcanic and tectonic features. The INL is outlined in blue with a black inset showing the location of the GRRA. Double lines indicate the location of a blow-up geologic map (Figure 11). The geologic base map is from Lewis et al. (2012). Shades of green, blue and purple illustrate late Precambrian to Paleozoic sedimentary rocks exposed in Basin and Range horst blocks north and south of the plain. Faults having late Neogene to Recent activity are shown in bold lines (after Anders et al., 2014). Pale shades of grey on the Snake River Plain indicate Quaternary basalt lavas (Holocene in darker shade); pale yellow indicates Quaternary sediment. Yellow = Quaternary cryptodomes, lava domes and volcanic fields consisting of geochemically evolved mafic to rhyolitic composition (e.g., McCurry and Welhan, 2012). Bold red colors indicate exposures of rhyolites (mostly ignimbrites) exposed along the margins of the plain. Major rhyolite volcanic fields are illustrated with bold dashed lines; HVF = Heise volcanic field. Twin Falls and Picabo fields overlap in age and are therefore combined. Deep boreholes are shown as red dots (Km=Kimberly; Ki+Kimama; SC=Sugar City; after Shervais et al., 2013). Boreholes located within the boundaries of INL are distinguished in Figures 5 and 11A. Inferred caldera locations and ages are illustrated with solid (better defined location) and dashed (less well defined location) black lines. TF=Twin Falls, after Shervais et al., 2013; MR=Magic Reservoir, after Leeman, 1982b; AF=American Falls, LCC=Little Chokecherry Canyon, KC=Kyle Canyon, LRS=Lost River Sinks, are after Anders et al., 2014; AV=Arbon Valley (or Taber), after Kellogg et al., 1994; Kuntz et al., 1992; McCurry, 2009; WT=Walcott, BCT=Blacktail Creek, Kilgore, and CC=Conant Creek, are after Morgan and McIntosh, 2005, modified by Anders et al., 2014; WC=Wolverine Creek, Ek=Elkhorn Spring, are after Anders et al., 2014). 2B. A cross-section of the crust and upper mantle (from McCurry and Welhan, 2012; modified from Peng and Humphreys, 1998). The cross-section extends southeast from the southern end of the Lost River Range to China Hat. ESRP = Eastern Snake River Plain; BVF = Blackfoot Volcanic Field; PMs = late Precambrian to Paleozoic miogeoclinal sedimentary rocks.

The YSRP is defined on the basis of a northeast trending, time-transgressive pattern in the inception of voluminous rhyolite volcanism (e.g., Armstrong et al., 1975; Pierce and Morgan, 1992). It 'migrates' at an average rate and in a direction closely mirroring 'absolute'

motion of the North American lithosphere (e.g. Smith et al. 2009) (Fig. 1). Volcanic fields evolved in waxing-waning cycles lasting several m.y., and overlapped in time and space with strong subsidence (sagging) along the volcanic track, and robust extension via Basin and Range extension in regions peripheral to the track. Detailed study of structures along the northern margin of the plain (Fig. 3) indicate 5 to 6 km of ESRP directed subsidence, almost all of which is accommodated by flexure (e.g., McQuarrie and Rodgers, 1998; Rodgers et al., 2002). Geophysical studies indicate that the subsidence occurred in response to intrusions on mafic magmas from the mantle into the lower- and middle-crust (e.g., Brott et al., 1981; Braile et al., 1982).

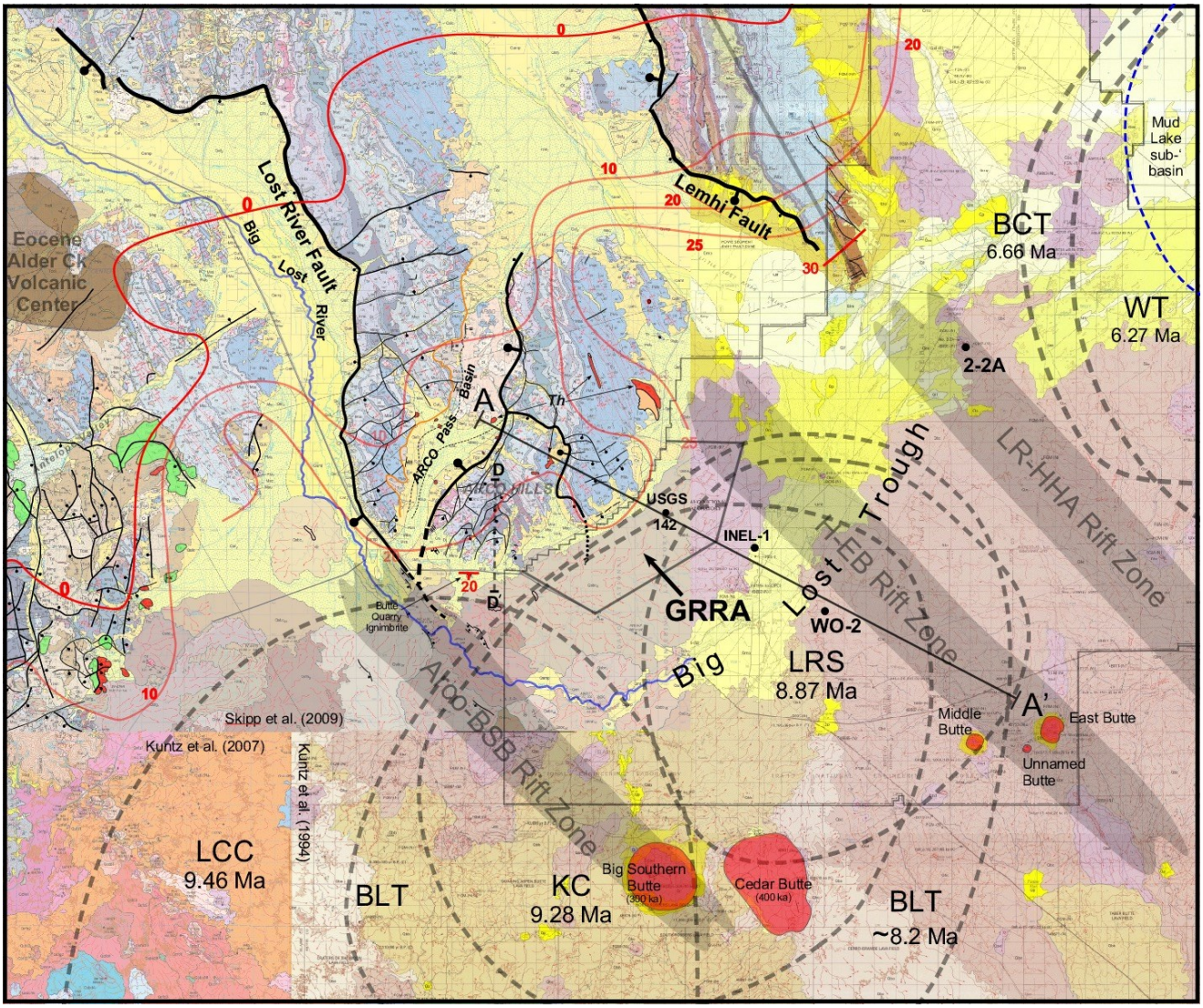

Figure 3. An intermediate scale geologic map of the GRRA and surroundings. Three base geologic maps are tiled together in the figure (Skipp et al., 2009; Kuntz et al., 2007; Kuntz et al., 1994). Neogene and Quaternary faults are highlighted in black; Quaternary rhyolite lava domes and cryptodomes in red shade. Picabo age and Heise age ignimbrites are also highlighted (in green and red colors, respectively). The geology base map is overlailn by inferred calderas (bold dashed lines); outlines of the Big Lost Trough basin and Mud Lake sub-basin are shown in thin dashed lines; red lines (red dots are measurement locations) that contour the tilt of Laramide fold axes into the plain (after Rodgers et al., 2002; McQuarrie and Rodgers, 1998); shaded regions illustrate volcanic rift zones; locations of deep boreholw (USGS142, INEL-1, WO-2 and 2-2A). The map also shows the locations of three project cross-section AA'.

Rhyolite fields may have cumulative volumes of 10,000-20,000 km^3 (e.g., Bonnichsen et al., 2008; Ellis et al., 2013). Volcanism is dominated by eruption of distinctively hot, relatively dry 'high grade' ignimbrites summarized by Branney et al. (2008) as SR-type, and voluminous lava flows. Similarities among the ignimbrites has made correlation, and therefore estimates of sources and volumes difficult, however recent work suggests that eruptions of >100 km^3 were not unusual. Many, but possibly not all (cf. Ekren et al., 1984), are sourced from caldera complexes. Assuming the cryptic volcanic fields (now largely buried by younger basalts) have evolved in a manner similar to Yellowstone caldera system, and to other large volcanic field world-wide, it seems likely that the fields host numerous overlapping and nested calderas. A prominent role for nesting of calderas is also strongly suggested by remarkably light patterns of oxygen stable isotope chemistry of the rhyolites (Bindeman et al., 2007; Watts et al., 2011; Drew et al., 2013).

Cessation of rhyolite volcanism was followed soon after by eruption of basalt lavas, beginning at ~6 Ma in the CSRP and ~4.2 Ma in ESRP (Shervais et al., 2013; Potter, 2014; Champion et al., 2002). The basalt eruptions produced a widely distributed basalt-dominated field consisting of hundreds of coalescing shield volcanoes (e.g., Greeley and King 1977; Kuntz et al., 1992; Hughes et al., 2002), having a cumulative volume of over 10,000 km^3 (e.g., McCurry et al., 2008). Accumulation of the basalts and concomitant subsidence of ESRP produced a basalt-dominated basin up to ~2 km deep (Shervais et al., 2013; Potter, 2014).

A number of spatially systematic patterns occur within ESRP basalt field (e.g., Kuntz et al., 2002, 1992; Hackett and Smith, 1992; Hughes et al., 2002; Wetmore et al., 2009) (Fig. 3). Many linear vents, alignments of vents and fracture systems trend to the northwest across parts of the ESRP, and west-northwest in the Spencer-Kilgore region south of the Centennial Range (e.g., Kuntz et al., 1992). Some of these features cluster into diffuse linear, northwest trending zones, and are identified as volcanic rifts zones (e.g., Kuntz et al., 1992, 2002; Rodgers et al., 2002). Some of these appear to merge into range bounding normal faults (e.g., Arco-Big Southern Butte Rift Zone, Figure 3), and may be dominantly tectonic in origin. Others may root into robust dike swarms (e.g., Parsons et al., 1998; Kuntz et al., 2002; Rodgers et al., 2002, 1990). The 'Great Rift' is the youngest and most prominent of these (e.g., Holmes et al., 2008). Interestingly, the Great Rift exhibits a systematic change in trend from northwest to northerly (Fig. 2), likely reflecting a northward change in the direction of regional strain (e.g., Payne et al., 2012). Other patterns in the distribution of volcanic vents have produced diffuse linear and curvilinear constructional topographic highs (e.g., 'Axial Volcanic Zone'; Fig. 3).

Basalt lavas are commonly interlayered with clastic sediment derived from drainage off ranges bounding the plain (e.g., Bestlin et al., 2002; Geslin et al., 2002). Importantly, accumulations of basalt and sediment in the central and eastern Snake River Plain have largely buried the underlying rhyolitic rocks and caldera systems. Virtually no unambiguous rhyolite sources are exposed, aside from those in the Yellowstone area (including Island Park). Volumes and sources of rhyolites in those regions are therefore inferred almost entirely from spatial distributions and depositional features of ignimbrite and fall deposits marginal to the plain, a small number of deep boreholes, and geophysical surveys.

In the ESRP eruptions of primitive basalts overlap in time and space with eruptions of comagmatic, highly geochemically evolved rocks, varying from Fe-enhanced and alkaline basalt to rhyolite (McCurry et al., 2008; Shervais et al., 2006; Leeman, 1982). These have produced a number of domes and cryptodomes across the ESRP such as Big Southern Butte and Middle Butte (Fig. 3), and evolved lava fields (e.g., Craters of the Moon, Cedar Butte, Unnamed Butte; Fig. 2, 3). Unlike the primitive basalt, parental magmas to these rocks underwent strong intracrustal fractional crystallization (e.g., Putirka et al., 2009, Whitaker et al., 2008) and remelting (e.g., Shervais et al., 2006; Bindeman et al., 2014). Hot cumulates associated with the long-lived active COM system (e.g., Kuntz et al., 1986), and voluminous young BSB system (e.g., McCurry et al., 2008), or possibly other cryptic (blind) systems across the ESRP, may be associated with localized thermal anomalies that are masked by the shallow active ESRP aquifer (e.g., McCurry and Welhan, 2012).

3. GEOPHYSICAL FRAMEWORK

Geophysical surveys have defined major features of the heat flow, crustal architecture, dynamics, seismicity, relative temperatures and distribution of fluids in the crust, lithosphere and deep mantle the YSRP region (e.g., Brott et al., 1981; Braile et al., 1982; Smith et al., 2009). Some aspects of these features are rapidly evolving as new EarthScope and GPS data continue to be gathered and interpreted (e.g., Payne et al., 2013). Some salient features are summarized here.

Numerous geophysical studies document prominent geophysical anomalies occur within the upper mantle and lower crust along the YSRP (e.g., Smith et al., 2009). Schmandt et al. (2012) identify low V_p and V_s seismic velocities extending from beneath Yellowstone to a depth of at least 1000 km. A prominent corridor of low velocity mantle also extends from the base of the crust to a depth of ~200 km along the entire ESRPA, lessening in magnitude from northeast to southwest beneath CSRP.

Kelbert et al. (2012) document a prominent region of low resistivity in the upper mantle beneath the ESRP, between 40 and 80 km depth. They interpret this as being produced by mantle containing 1-3% partial melt, comparable to melt fractions inferred from shear wave velocity (e.g., Wagner,2010; Schmandt et al. 2012). They also infer that mantle derived fluid may be preferentially rising into the lower crust preferentially along the margins of the ESRP. Interestingly, they also infer decoupling in the resistivity and seismic tomography data beneath Yellowstone indicating that the mantle under Yellowstone is depleted in fluid (magma), relative to regions of mantle under ESRP. Zhdanov et al. (2012; 2011) also infer low resistivity of upper mantle and lower crust beneath the SRP. However, in contrast to Kelbert et al., they also infer a plume-like region of low resistivity beneath Yellowstone. These and other regional geophysical surveys are compelling evidence for existence of melt, likely basaltic in composition, in the upper mantle and lower crustal regions of ESRP. It is plausible that the mantle underlying ESRP has been at or near its solidus (~1300°C) for the last 10 m.y.

Figure 4 illustrates a large-scale conceptual cross-section of the ESRP and surrounding regions that is based mainly upon the seismic and gravity model of Peng and Humphreys (1998). These authors build upon seismic and gravity work done in the 1970's and 1980's (e.g., Braile et al., 1982; Sparlin et al., 1982; Greensfelder et al., 1982; Smith and Braile, 1994). The model illustrates a crustal structure that is dominated by mafic lower crust, felsic crystalline upper crust and several kilometers of supracrustal rocks (the Cordilleran Miogeocline). Rocks directly beneath the ESRP are distinguished by presence of a mid-crustal region of unusually high density and a thin layer at or near the Moho that contains a significant fraction of melt.

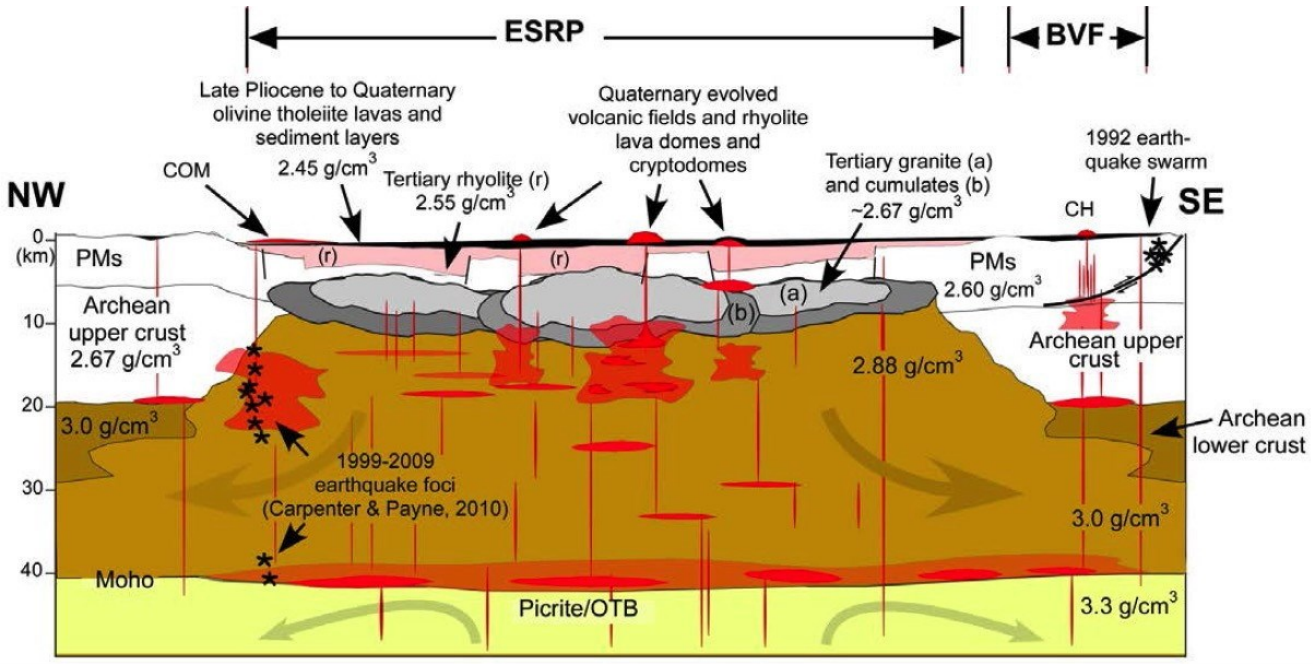

Figure 4. A cross-section of the crust and upper mantle (from McCurry and Welhan, 2012; modified from Peng and Humphreys, 1998). The cross-section extends southeast from the southern end of the Lost River Range to China Hat. ESRP = Eastern Snake River Plain; BVF = Blackfoot Volcanic Field; PMs = late Precambrian to Paleozoic miogeoclinal sedimentary rocks.

Importantly, the prominent mid-crustal density anomaly underlying the ESRP is inferred to be a product of intrusion of dense, hot (~1300°C) mantle derived melts (basalt) into pre-existing mid-crustal rocks (e.g., Brott et al., 1981; Smith and Braile, 1994). These initiated petrologic processes that culminated with eruption of rhyolite and intrusion of granitic rocks (e.g., Christiansen and McCurry, 2008; Szymanowski et al., 2015). McCurry and Rodgers (2009) applied a Nd- isotopic tracer method to extruded rhyolites as a method of inferring the original amount of mantle derived mass added to the crust, equating to a layer of gabbro ~14 km thick. Leeman et al. (2008) independently arrived at a similar estimate based on an energy balance analysis. Absence of a significant deviation of crustal thickness beneath ESRP, led Rodgers and McCurry (2009) to infer that the excess mass was transferred via lower crustal flow into regions marginal to the plain. This idea is supported in more recent geophysical work by Yuan et al. (2010); it is also consistent with geophysical work by DeNosquio et al. (2009) indicating that the mid-crustal 'sill' extends up to ~40 km southeast of the ESRP.

Geophysical constraints for the ESRP upper crust architecture include long baseline active seismic refraction (e.g., Sparlin et al., 1982; Braile et al., 1982) and resistivity (Zohdy and Stanley, 1973) surveys, and a seismic refraction survey focused on the northern margin of the ESRP (Pankratz and Ackermann, 1982). The seismic refraction and resistivity surveys indicate a steeply dipping northern, fault-like boundary to the ESRP, south of the Arco Hills and beneath GRRA, and consistent with a caldera margin in that region.

Interpretations of upper crustal structures from seismic, gravity and magnetic surveys data are complicated in the ESRP and CSRP regions by occurrence of interlayered basalts and sediment (e.g., Liberty et al., 2015). Josten and Smith (1997) analyzed Bouguer gravity data in the ESRP and inferred regions of likely buried calderas in the ESRP where low density, rhyolitic caldera fill plausibly abuts against higher density Paleozoic carbonate rocks.

4. GEOLOGY OF THE GRRA AREA

The surficial geology of the GRRA and vicinity are illustrated in Figures 3. Rocks exposed in the Pioneer, Lost River and Lemhi Ranges north of the plain are dominantly Paleozoic carbonate and siliciclastic rocks (purple and blue colors) that are deformed and cut by Sevier and Laramide folds and faults. The Paleozoic rocks are unconformably overlain by Eocene volcanic and volcaniclastic rocks of the Challis Formation (brown and tan colors). The closest of these, the Alder Creek complex, is located about 30 km northeast of GRRA. Distal sedimentary facies of that system are exposed in the Arco Pass basin, 5 km north of GRRA (Fig. 5). Eocene and older rocks underwent diachronous periods of late Eocene to early Oligocene and Miocene to Recent extension and related normal faulting. Oligocene extension is evident in a half graben in the Arco Hills (Arco Pass basin). The graben contains tilted Eocene Challis formation and an older gravel formation. These are overlain by less strongly tilted to nontilted gravels and thin discontinuous valley fill erosional remnants of ignimbrites of the Heise volcanic field in the Arco Hills and Picabo and Heise groups in the Pioneer and Lemhi Mountains. The graben bounding Arco Pass fault trends to the south-southwest, and apparently intersects with the active Lost River Fault near the town of Arco. A branch of the Arco Pass fault extends to the south, bisecting the Arco Hills, projecting to the south beneath the GRRA. However, there is no evidence for Miocene or younger offset on that fault.

Miocene to Recent normal faulting has produced the current fault block physiography of the region. Prominent range bounding active normal faults include the Lost River and Lemhi Fault systems (e.g., Janecke et al., 1993; Bruhn et al, 1992; Wu and Bruhn, 1994). The

Lost River fault projects to the south into a diffuse system of small-offset normal faults referred to as the Arco Rift Zone (e.g., Kuntz et al., 1992; Kuntz and Cork, 1978; Jackson et al., 2006).

McQuarrie and Rodgers (1997) and Rodgers et al. (2002) document progressive southward tilting of originally horizontal late Mesozoic fold axes and in volcanic and volcaniclastic deposits of the Heise volcanic group. Tilt contours are illustrated in Figure 3. These structures document ~20 km wide zone marginal to the ESRP in which tilts increase from zero to 20-30 degrees to the south, accommodating 4.5 to 8.5 of subsidence of the plain, most which occurred ~10 and 8.5 Ma in the GRRA area. Minor east-northeast trending normal faults are inferred to have been produced by flexure of the brittle crust. Contour reentrants coincide with major Quaternary grabens indicating that the reentrants are artifacts of Quaternary faulting and basin formation.

The southernmost ends of the Pioneer, Lost River and Lemhi Ranges are cut by an unusually high density of small-offset, crosscutting normal faults (Fig. 3). Bruhn et al. (1992) indicate that those in the southern Lemhi Mountains are a product of complex fault tip evolution of the Lemhi fault (e.g., their Figure 10). Morgan (1984) suggested that some of the small faults could be related to normal fault ring fracture zones bordering calderas that may reside a short distance to the south of the ranges.

Quaternary structures in the GRRA area are dominantly northwest trending. However, proposed cryptic calderas clustered near the southern margin of the Lost River Range imply existence of related cryptic curvilinear ring fault systems beneath basalts, perhaps 10's km long and several kilometers deep. Some of these are likely to have orientations that intersect at high angles with Quaternary structures.

Basalt lavas produced mainly from overlapping shield volcanoes dominate areas south of the mountain ranges. Surficial basalts near GRRA vary in age from ~300 to ~200 ka (Skipp et al., 2009) and do not appear to have significant tectonic tilt. Near the ranges the basalts feather out and are interbedded and discontinuously overlain by range derived clastic sediment. Sediment interbeds also commonly occur in borehole cores and logs (e.g., Bestland et al., 2002; Geslin et al., 2002). Most appear to record transient fluvial, lacustrine and eolian processes. However sedimentation associated with the Big Lost Trough (Fig. 3) appear to have been unusually robust and long-lived. Current drainage into that system includes the Big Lost River, Little lost River and Birch Creek. The largest, the Big Lost River, has an unusual drainage pattern defined by southward flow from the Big Lost Graben, followed by deflection to the east and then north by constructional volcanic features of the 'axial volcanic zone'. Based upon borehole studies, sedimentation associated with that system occurs to at least 2.5 Ma (e.g., Geslin et al., 2002).

Hundreds of boreholes have been drilled across INL, focused on defining stratigraphic and structural features relevant to understanding the hydrogeology and hydrochemistry of the ESRP aquifer, and for monitoring fate and transport of site related contaminants (e.g., Bartholomay and Twining, 2015; Champion et al., 2011). Many of the boreholes have core samples, almost all have downhole geophysical logs (most importantly gamma logs). These have been used to produce detailed subsurface correlation maps of basalt and sediment interbed layers, typically to depths of ~200 meters (e.g., Figure 4B, C). Significant results of these studies include, 1. documentation of spatial distribution of lava accumulation rates, 2. long term existence of the Big Lost Trough, 3. little or no tilting of basalt layers up to at least ~1 Ma, 4. little or no faulting, 5. Little or no systematic time sequential change in basalt lava chemistry that are characteristic of waning phases of hot spot activity.

4.1 Deep borehole geology

Several boreholes penetrate through the entire basalt section in the GRRA and INL area, INEL-1 (to 3.16 km), WO-2 (to 1.52 km), 2-2A (to 910 m), and most recently USGS 142 (to 573 m). Other regional deep boreholes include those of Project Hotspot (Kimberly, to 1958 m, and Kimama, to 1912 m; e.g., Shervais et al., 2013; Potter, 2014), and the Sugar City borehole (Embree et al., 1978). The Kimberly borehole penetrates 1350 m of homogeneous, intracaldera-like rhyolite (Knott et al., 2013) and referred to by Shervais et al. (2013) as the 'Twin Falls caldera'.

Summaries of salient aspect of borehole stratigraphy near GRRA are illustrated in Figure 5. Rhyolites exposed in boreholes WO-2 (e.g., Anders et al., 2014; McCurry and Rodgers, 2009) and 2-2A (Dougherty, 1979) are dominated by two rhyolite lava flows, and thin outflow ignimbrites (i.e. deposited outside of their source calderas) of the Heise volcanic field. The WO-2 borehole bottoms-out in one of the most voluminous Heise ignimbrite units (the Blacktail Creek tuff), but it is not clear whether it is within or outside of a source caldera.

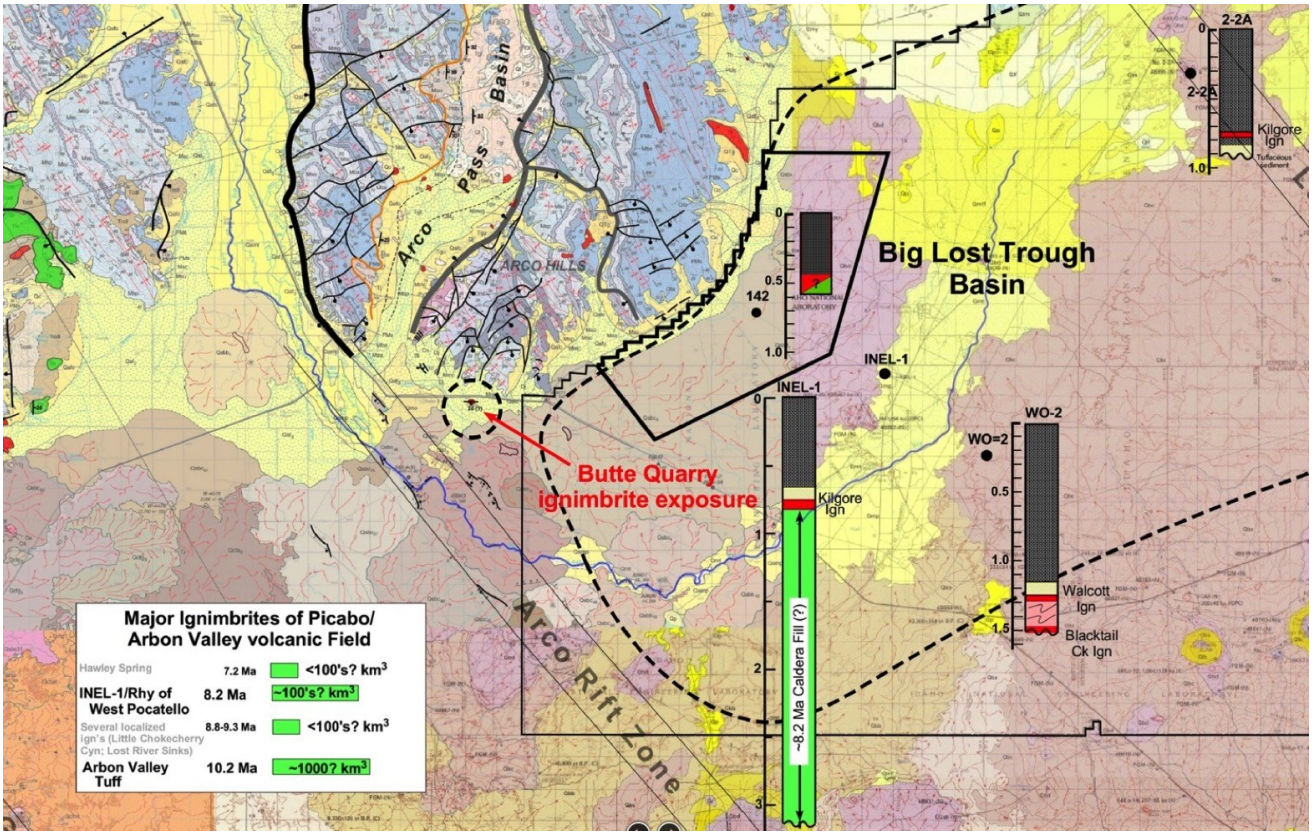

Figure 5. Summary map illustrating volcanic rock stratigraphy observed in boreholes INEL-1, 2-2A, WO-2 and USGS 142. Green: rhyolite correlated with the Picabo volcanic field; red: rhyolite correlated with the Heise volcanic field.

The INEL-1 borehole penetrates ~2.5 km of rhyolite below of basalt cover of ~750 m (total depth of ~3.2 km). Rhyolite sampled at ~770 m may correlate to outflow facies of the Tuff of Kilgore (McBroome et al., 1981; cf. Anders, et al., 2014).

Importantly, three cored intervals from INEL-1, extending over a range of depth of 1.1 to 3.2 km, yielded rhyolites containing zircon phenocrysts having overlapping U-Pb SHRIMP dates of ~8.2 Ma (McCurry and Rodgers, 2009; Drew et al., 2012). Phenocryst textures of these rocks are typical of SR-type rhyolite (after Branney et al., 2008). Drew et al. (2012) point out that rhyolite at ~1.5 km depth bears striking geochemical similarities to a possible lavalike ignimbrite near Pocatello (Rhyolite of West Pocatello). They suggest that they may be correlative parts of a particularly large ignimbrite. If the 8.2 Ma rhyolites of INEL-1 are extrusive, as seems likely, then they are clear evidence for existence of a Picabo-age caldera in the GRRA area (referred to here as the 'Big Lost Trough caldera').

Figure 5 illustrates a simplified lithologic log for recently drilled borehole USGS 142. This borehole is located near the center of GRRA, and therefore provides key stratigraphic control in that area to a borehole bottom depth of 573 m. The borehole penetrates 425 meters of basalt lavas, and lesser amounts of sediment interbeds. However the lower portion of the borehole penetrates through a single ignimbrite ~150 m thick. Petrographic examinations of core from upper and lower parts of the ignimbrite exhibit clear eutaxitic textures indicative of its pyroclastic origin. Interior parts of the ignimbrite exhibit banding and rheomorphic features that are typical of SR-type rhyolitic ignimbrites. Examination of variation in intensity of welding of the bottom-hole core suggests that the base of the ignimbrite occurs with a few meters of that depth. Preliminary examination of the bulk major and trace-element composition and petrography of the rhyolite indicates that it is not correlated to any of the large Heise ignimbrites. Dating and additional geochemical work on the rhyolite are in progress. The 150 m thick ignimbrite is thicker than most regional outflow ignimbrites. We speculate that the ignimbrite could be an upper cooling unit of the Big Lost Trough (BLT) caldera, perhaps from the same sequence that occurs in borehole INEL-1. However it could also be an outflow of the BLT caldera resting on country rocks, or an outflow unit of some as yet unidentified caldera that erupted soon after the BLT caldera, and that ponded within the moat region of the BLT caldera.

5. CALDERAS AND THEIR SIGNIFICANCE FOR EGS EXPLORATION IN ESRP

Calderas are perhaps the single most important structural and lithologic (rock materials) features of the ESRP with regard to its EGS potential (e.g., Podgorney et al., 2013; Moody and Plummer, 2014; Wohletz and Heiken, 1992). Key geologic requirements for successful FORGE development in GRRA include a rock reservoir that is shallow enough to drill to obtain necessary temperature (assumed to be in the 1.5 to 4 km depth range at GRRA), homogeneous (i.e. free of strong stratification, joint systems, foliations or other characteristics of rock anisotropies), voluminous, dense (i.e. low fracture density and low porosity) and dry. In a rhyolite dominated volcanic terrain such as YSRP the best fit for these criteria would be the intracaldera facies of a major ignimbrite eruption (e.g., Wilcock et al., 2013; Wohletz and Heiken, 1992).

We summarize the major features of caldera systems, including relevant aspects of their nomenclature, classification, and formation, mainly following review papers by Branney and Acocella (2015), Acocella (2006; 2007), Cole et al. (2005), and Lipman (1997). We then summarize a rationale for inferring existence, sizes, depths and locations of numerous cryptic calderas that underlie basalts across ESRP (e.g., Anders et al. 2014; Morgan and McIntosh 2005).

5.1 Caldera systems

Calderas are subsided regions that form in response to rapid, voluminous magma transfer from shallow (upper crust) magma reservoirs (Branney and Acocella, 2015). Five end-member types of calderas are widely recognized (e.g., Lipman 1997; Cole et al. 2005), including Piston, Piecemeal, Trap-door, Downsag and Funnel (Figure 6). Most large explosive eruptions ≥ ~10 km^3 produce calderas. However some may not (Ekren et al. 1984). Additionally, some calderas are non-eruptive, collapse being brought about by lateral transfer of magma within laterally extended magma reservoirs (Lipman 2008). Correlated patterns between caldera area, caldera depth and erupted magma volumes have been defined by studies of young calderas in diverse geologic environments (e.g., Acocella, 2007; Gregg et al., 2012). Eruptions of 100's to 1000's km^3 (common along the YSRP) typically produce calderas 20 to 50 km across and 1-3 km deep.

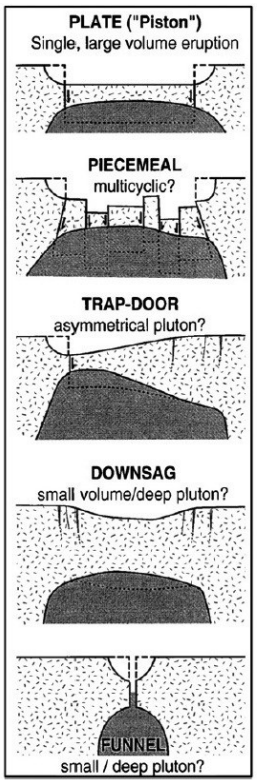

Figure 6. Types of calderas and caldera classification (from Acocella, 2006).

Development of large silicic explosive-volcanism-related calderas generally represent the climax of activity of regionally extensive volcanic fields (e.g. Lipman et al., 2015). These volcanic systems evolve through a waxing and waning sequence of events lasting ~10^4 – 10^6 years and referred to and described by Smith and Bailey (1968) as the 'resurgent-cauldron cycle' and subsequently elaborated on and modified in numerous subsequent studies (e.g., Walker, 1984; Lipman, 1997; Cole, 2006; Acocella, 2006, 2007).

Activity begins with development of a precaldera volcanic field consisting numerous small and compositionally diverse volcanoes. Incremental assembly of a magma reservoir at depths of ~5-10 km leads to eventual catastrophic eruption via reverse ring fracture systems up to 10's kilometers long. Ring fractures generally conform to the shape of the underlying magma reservoir(s), but may also be affected by pre-existing structures and regional stresses. Explosive jetting from the vents produces hot fragmental volcanic debris that collapses back to ground as pyroclastic density currents (PDC) (e.g., Wilcock et al., 2013) that incrementally produce deposits referred to as ignimbrites. Many of the PDC's infill into the subsiding caldera depression, and may rapidly accumulate to thickness of a kilometer or more, exceeding the thickness of coeval ignimbrites formed beyond the margins of the caldera by a factor of 10 or more. Owing to their rapid accumulation near source vents the resulting intracaldera deposit is generally massive and densely welded.

Calderas produce patterns of structures and deposits. Acocella (2006, 2007) describes four time sequential stages of evolution. Caldera development begins with downsagging (stage 1), followed by formation of reverse ring-fracture faults along which most magmas are erupted (stage 2), followed by additional downsagging (stage 3) and finally collapse of roof wall rocks via a system of normal ring

faults (stage 4). Over-steepened walls of normal fault scarps produces a 'collar structure' consisting of scalloped shaped landslide scars, and landslide debris into the caldera as mega- and mesobreccia. Collar zones and regions of sagging and incipient collapse-related normal and reverse faults may occur in a zone up to kilometers outside of the ring-fracture and vent systems for the caldera. Major caldera-bounding ring fracture faults and related vents are curvilinear and may be ~10's km long in the largest calderas. Intracaldera vents may be linear, curvilinear or complex.

Postcaldera activity commonly involves strong hydrothermal alteration of caldera fill owing to capture of meteoric water into the caldera depression and shallow heat sources. This may be a particularly robust process in YSRP caldera systems as suggested by occurrence of remarkably light $\delta^{18}O$ of latter erupted rhyolites relative to those erupted earlier in nested caldera fields (Bindeman et al., 2007; Watt et al., 2011; Drew et al., 2013).

Post-collapse activity also commonly includes extrusion of degassed rhyolite magma along ring-fracture faults, deposition of lacustrine and fluvial sediment within the caldera, and in the case of many large calderas uplift of central regions of the floor of the caldera ('resurgent doming'; e.g., Kennedy et al., 2012) by intrusion of sills (e.g., Fridrich et al., 1991; Kawakami et al. 2007) or by renewed deeper intrusive activity by nonerupted remnants of the underlying magma body (e.g., Lipman 1984; Smith and Bailey 1968; de Silva et al., 2015). Uplift commonly produces radial and linear normal fault systems. Multiple resurgent domes are formed with some very large calderas (e.g., San Juan and Yellowstone calderas, e.g., Christiansen, 2001; Casadevall and Ohmoto, 1977). These may be connected by systems of normal faults and fractures (Christiansen, 2001; Casadevall and Ohmoto, 1977. CCDB proposes a detailed nomenclature for calderas based upon key aspects of post-caldera activity (Geyer and Marti, 2008). Figure 7 illustrates a simplified integrated model of a caldera (Branney and Acocella 2015).

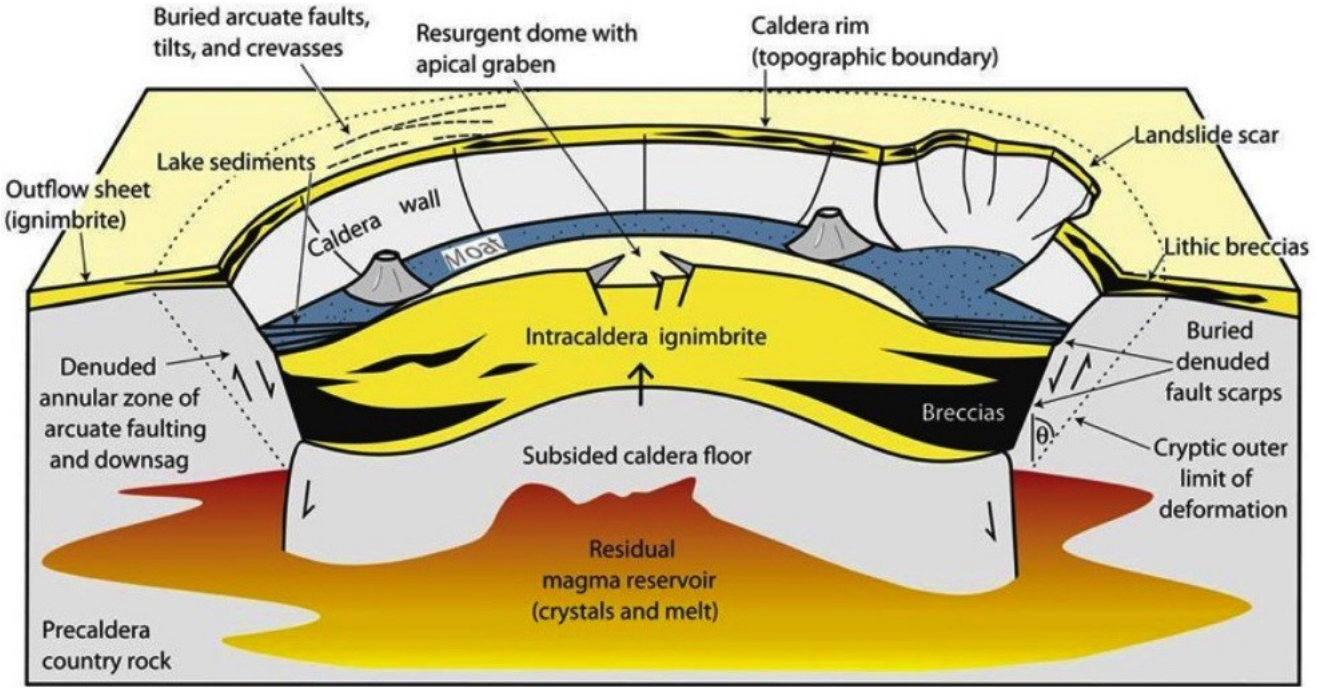

Figure 7. A conceptual model of a resurgent caldera (after Branney and Acocella (2015). The region labeled "Denuded annular zone of arcuate faulting and downsag" and with lanslide scars is equivalent to the 'collar zone' of Lipman (1997).

Major silicic volcanic fields commonly form complex overlapping, 'nested', calderas . These differ from piecemeal calderas in that they form in diachronous events that may be hundreds of thousands to millions of years apart in time (e.g., Lipman, 1997; Christiansen, 2001). Nesting may produce cumulative subsidence of many kilometers. Caldera nesting occurs in the Yellowstone volcanic field (Christiansen et al., 2001). Volcanological (e.g., Morgan and McIntosh, 2005; Anders et al., 2014) and geochemical studies (Bindeman et al., 2007; Watts et al., 2011; Drew et al., 2013) suggest that it is a also common feature of other parts of the YSRP volcanic track.

5.2 Criteria for identifying and locating cryptic (buried) calderas

Inference of cryptic calderas in the central and eastern Snake River Plain have been made on the basis of:

1. Correlation, and volcanic facies and kinematic analyses of caldera-related volcanic materials, mainly ignimbrites and ring-fracture lava flows (e.g., Anders et al. 2009, 2014; Morgan and McIntosh, 2005; Morgan et al., 1984, 2008; Morgan, 1988, 1992; Kellogg et al., 1994; Prostka and Embree, 1978; Embree et al., 1982);

2. Caldera-related structures including an inferred resurgent dome (Morgan and McIntosh, 2005) and possible caldera-related normal and collar faults (e.g., Morgan et al. 1984; Morgan,1988);

3. Studies of deep boreholes that penetrate through shallow basalts into the underlying rhyolites (e.g., Doherty et al., 1979; McCurry and Rodgers, 2009; Anders et al., 2014);

4. Spatial distributions of basalt and rhyolite lava dome vents (e.g., Doherty et al., 1979; Kuntz and Dalrymple, 1979; Kuntz, 1992);

5. Persistent regions of sediment accumulation (e.g., Kuntz et al., 1992);

6. Seismic surveys (Pankratz and Ackermann, 1979: Braile et al., 1982; Sparlin et al. 1982);

7. Resistivity surveys (Zohdy and Stanley, 1973);

8. Interpretations of gravity and magnetic anomalies (Josten and Smith, 1997; Mabey, 1978, 1982).

5.3 Distribution of calderas in ESRP (Picabo and Heise volcanic fields)

Figures 2 and 3 illustrates the inferred locations of calderas in the ESRP. Dashed lines are intended to encompass source vents for the respective calderas; they do not distinguish between caldera wall, and normal and reverse ring fault systems (Fig. 6). Existence and locations of calderas follow mainly from previous syntheses by Anders et al. (2014), Shervais et al. (2013), Morgan (1984, 1988), and Morgan and McIntosh (2005). Examinations of deep boreholes indicate that calderas associated with the Heise volcanic field (≤6.66 Ma) are located to the east of borehole INEL-1 and likely east of borehole WO-2. Three of the cluster of four nested calderas shown in the GRRA area (Fig. 3) are inferred from relatively small erosional remnants of outflow ignimbrites in the southern Pioneer and White Knob Mountains (Anders et al., 2014). The locations and sizes of those calderas are therefore weakly constrained and may differ by many kilometers from the boundaries shown in the figure. A fourth caldera, referred to here as the Big Lost Trough caldera, is added to the Anders et al. (2014) map. This caldera is a modification of the INEL-1 caldera proposed by Dougherty et al. (1979), and is inferred from previously described seismic refraction (Pankritz and Ackerman, 1982) and resistivity surveys (Zohdy and Stanley, 1973), and deep boreholes (INEL-1 and USGS 142). We suggest that it is also broadly coincident with, and likely has contributed to the existence of the Big Lost Trough sedimentary basin. The northern boundary of the outer wall of this buried caldera may be accurate to within a kilometer, based largely upon seismic refraction work by Pankratz and Ackermann (1982).

6. GRRA STUDY AREA: A PRELIMINARY CROSS-SECTION INTERPRETATION

Figure 8 illustrates a northwest-southeast cross-section of the GRRA and surroundings.

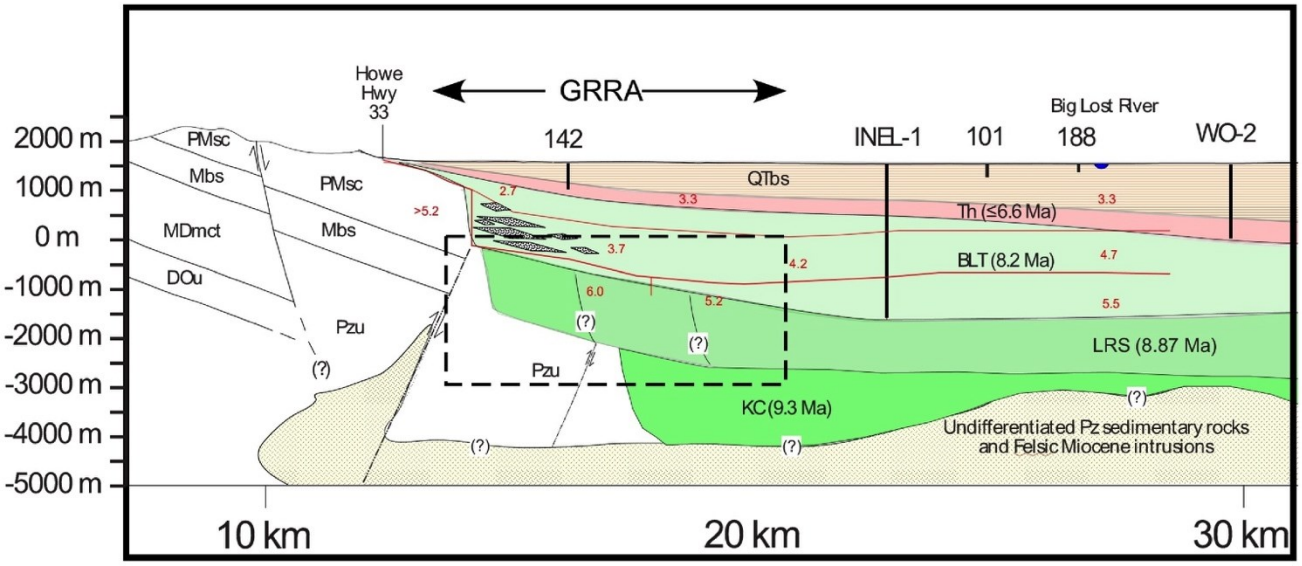

Quaternary-Late Neogene

Qalf - alluvial and fluvial deposits (includes Qc - colluvial deposits)
Qr - rhyolite lava dome (Pleistocene)
QTg - gravels, glacial and other sources (Holocene to Pliocene)
QTbs - basalt of the ESRP (Holocene to Pliocene)
Th - Heise group rhyolite ignimbrites (6.66 to 4.5 Ma)
BC - Blacktail Creek ignimbrite of Heise group (6.66 Ma)
Tp - Picabo group rhyolite ignimbrites (10.2 - 7.7 Ma)
BLT - 'Big Lost Trough' ignimbrite (~8.2 Ma)
LRS - Lost River Sinks ignimbrite (8.87 Ma)
KC - Kyle Canyon ignimbrite (9.28 Ma)
LCC - Little Choke Cherry ignimbrite (9.46 Ma)
TAV - Arbon Valley ignimbrite (10.2 Ma)

Tgu - upper gravel sediments (Miocene to Oligocene)
Tgl - lower gravel sediments (Eocene)
Tcv - Challis group volcanics (Eocene)

Paleozoic and Proterozoic sedimentary units

PMsc - Calcareous sandstones and limestones
Mbs - Quartzite, limestone and dolostones
MDmct - Siliceous sandstones, quartzite and limestones
DOu - Undifferentiated dolostone
OYu - Quartzites and calcareous sandstones

Figure 8. Blow-up view of the part of cross-section AA' (Fig. 3) near the GRRA. Numbers across the top of the figure indicate boreholes located close to the cross-section (mostly with USGS prefix). Faint red lines and numbers are model boundaries and seismic velocities from Pankhurst and Ackermann (1982). The dashed box illustrates the potential GRRA reservoir target zone (assumed to be 1.5 – 4 km depth). Stippled regions near caldera boundaries represent likely mega- and mesobreccia rich regions. Question marks indicate uncertainty in location of the deeper nested Picabo-age caldera boundaries. The diagram illustrates that USGS 142 penetrates into Th (Heise volcanics, undifferentiated). New geochemical data suggest that it is either an unknown Heise unit, or a Picabo unit.

Approach and uncertainties: Cross-sections are constrained by surface geology, borehole data and caldera locations as defined in the previous section. At present there are no unambiguous constraints for common features of calderas, such as structural collars, megabreccia zones, resurgent dome structures, moat deposits or hypabyssal intrusions (illustrated diagrammatically in Fig. 8). We therefore omit these from the cross-sections with the understanding that some or all of these are likely present.

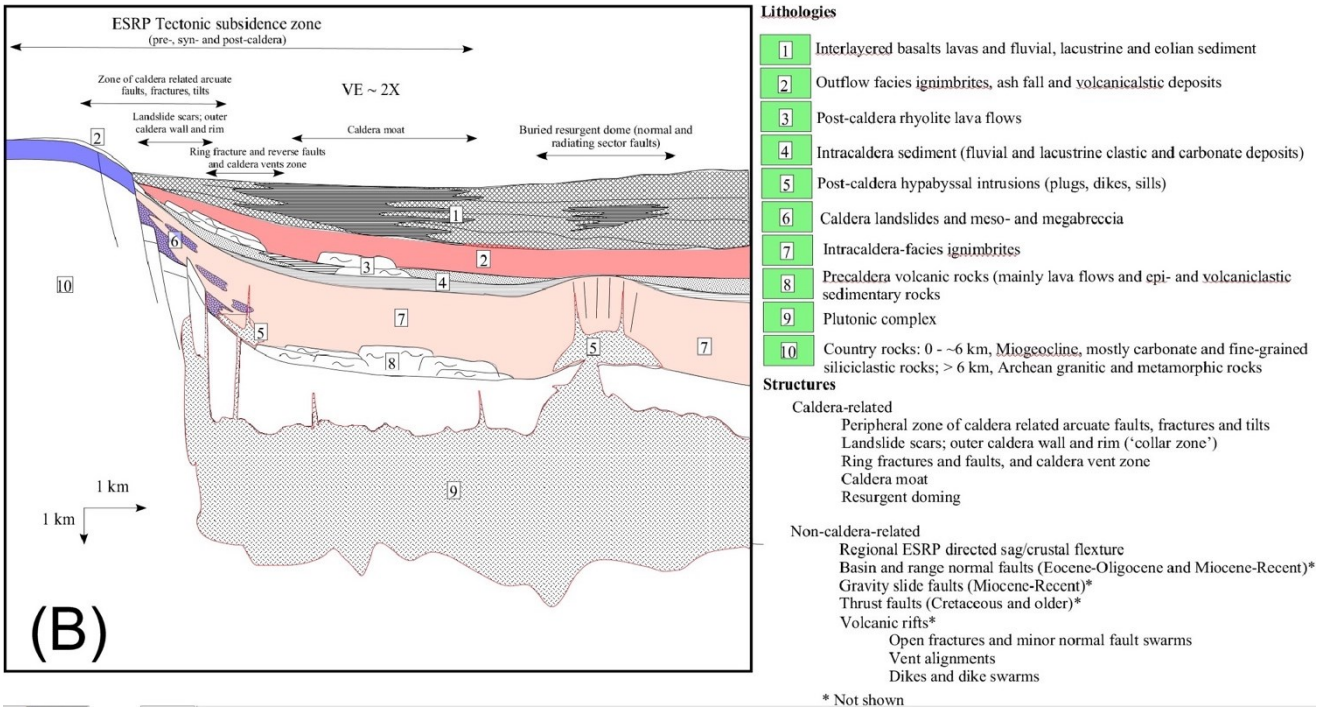

Figure 9. A conceptual model illustrating possible lithologies and structures in the GRRA area.

The cross-section extends from the Arco Hills to the southeast across the center of GRRA, It roughly parallels the seismic survey line of Pankratz and Ackermann (1982) and the resistivity survey of Zohdy and Stanley (1973). It also crosses close to three deep boreholes (USGS 142; INEL-1; and WO-2). It is therefore the best constrained cross-section currently possible for reservoir-depth interpretation. Long vertical red lines illustrate basalt vents that reach to modern surface. Faint red lines and red numbers illustrate the velocity model boundaries and modeled seismic velocities of Pankratz and Ackerman (1982). The diagram illustrates three nested calderas (KC - Kyle Canyon, LRS - Lost River Sinks and BLT). Each is assumed to contain ~1 km of caldera fill, and that the fill extends to the top of ring fracture normal faults. Deeper, older calderas (KC and LRS) are inferred to tilt more strongly into the plain than the young BLT caldera (following from subsidence timing constraints of Rodgers et al., 2002). We assume a total flexure-related subsidence of ~4 km (the minimum estimate of Rodgers et al., 2002). As illustrated in the Figure, host rocks are likely to be Picabo age intracaldera rhyolites. Thicker, more homogeneous reservoir rocks are more likely to occur beneath the southeastern parts of the GRRA.

6.1 GRRA Reservoir Hypotheses

Figure 10 illustrates plausible worst-case and best-case geologic conceptual model hypotheses for the proposed GRRA reservoir. The models are simplified to emphasize characteristics of the likely rhyolite-dominated reservoir rocks. Other details of rock lithologies and structures are neglected (cf. Figure 9). The 2-d conceptual models corresponds to cross-section AA', Figure 3.

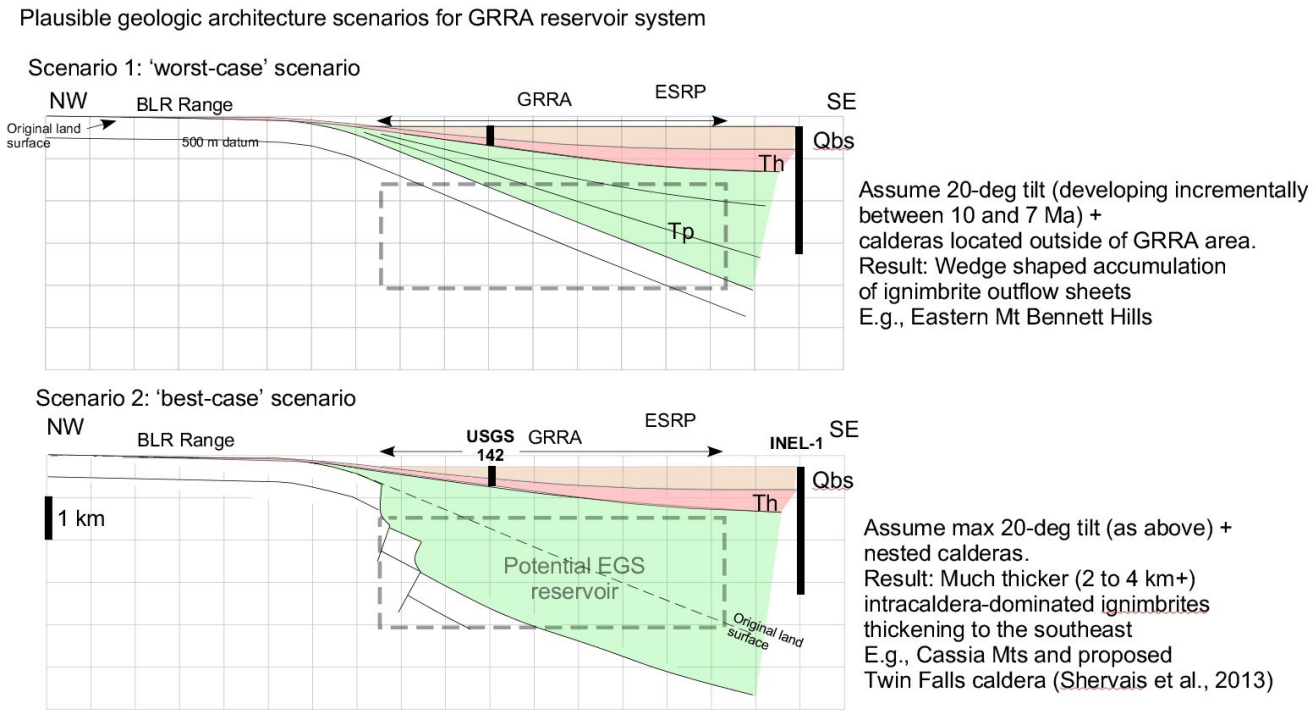

1. Worst-case: wedge of thin outflow ignimbrite sheets; thinning to NW, cumulative thickness decreasing roughly linearly from ~3 km under SE parts of GRRA to less than a few hundred meters under NW parts of GRRA.

2. Best-case: Deep nested calderas; overlapping or nearly overlapping narrow steep caldera walls and narrow collar; 2-4 km (or more if multiple nested calderas) of densely welded intracaldron ignimbrites. Other 'best case' features:

- minimal landslide mega- and meso-breccia
- 'moat region' of caldera; no resurgent doming, or resurgent dome located far enough away to neglect it
- narrow cooling break; minimal lacustrine or other intercaldera deposits
- little post caldera tectonic or volcanic and intrusive activity aside from incremental deposition of basalt lavas and sediment

Figure 10. This figure is intended to bracket a plausible range of subsurface architecture for the GRRA..

Worst case scenario: In the worst case scenario, caldera boundaries occur outside of the GRRA area. Basin development is solely a product of flexure subsidence of the plain. In this case rhyolites are dominantly outflow facies of ignimbrites (i.e. relatively thin and discontinuous). This model predicts that the southern half of GRRA would host potentially suitable reservoir host rocks.

Best-case scenario. In this scenario one or more nested caldera margins overlap close to the southern margin of the Arco Hills. Caldera collapse, enhanced by flexure tilting could produce thick, dense, homogeneous intracaldera reservoir rocks that encompass nearly the entire potential reservoir region. Seismic refraction data of Pankurst and Ackmann (1982), indicating a sharp drop in basement depth, suggests that this scenario may be closer to the actual case.

6. CONCLUSIONS

Preliminary 2-d modeling of the geologic and geophysical characteristics of the GRRA are consistent with a high probability of favorable types of EGS host rocks at potential reservoir depths of 1.5 to 4 km, particularly towards the southern and southeast parts of the GRRA. Reservoir depth rocks are likely to be dominated by marginal or moat, intracaldera ignimbrite-facies of caldera systems. Calderas are likely to be nested. Boreholes may therefore encounter diverse sedimentary deposits, lava flows or caldera collapse breccias between intracaldera ignimbrites.

The large potential magnitude of the EGS resource and unique combinations of favorable reservoir-depth host rocks and a shallow robust aquifer system indicate that GRRA is an ideal site for EGS research and development.

REFERENCES

Acocella, V., 2006, Caldera types: How end-member relate to evolutionary stages of collapse: Geophysical Research Letters, v. 33, no. 18, p. 2–6, doi: 10.1029/2006GL027434.

Acocella, V., 2007, Understanding caldera structure and development: An overview of analogue models compared to natural calderas: Earth-Science Reviews, v. 85, no. 3-4, p. 125–160, doi: 10.1016/j.earscirev.2007.08.004.

Acocella, V., Funiciello, R., Marotta, E., Orsi, G., and De Vita, S., 2004, The role of extensional structures on experimental calderas and resurgence: Journal of Volcanology and Geothermal Research, v. 129, no. 1-3, p. 199–217, doi: 10.1016/S0377-0273(03)00240-3.

Anders, M.H., Geissman, J.W., Piety, L.A., and Sullivan, J.T., 1989, Parabolic distribution of circumeastern Snake River Plain seismicity and latest Quaternary faulting: Migratory pattern and association with the Yellowstone hotspot: Journal of Geophyscial Research, v. 94, no. B2, p. 1589–1621, doi: 10.1029/JB094iB02p01589.

Anders, M.H., Rodgers, D.W., Hemming, S.R., Saltzman, J., Divenere, V.J., Hagstrum, J.T., Embree, G.F., and Walter, R.C., 2014, A fixed sublithospheric source for the late Neogene track of the Yellowstone hotspot: Implications of the Heise and Picabo volcanic fields: Journal of Geophysical Research: Solid Earth, v. 119, no. 4, p. 2871–2906, doi: 10.1002/2013JB010483.

Anders, M.H., Saltzman, J., and Hemming, S.R., 2009, Neogene tephra correlations in eastern Idaho and Wyoming: Implications for Yellowstone hotspot-related volcanism and tectonic activity: Bulletin of the Geological Society of America, v. 121, no. 5-6, p. 837–856, doi: 10.1130/B26300.1.

Armstrong, R.L., Leeman, W.P., and Malde, H.E., 1975, K-Ar dating, Quaternary and Neogene volcanic rocks of the Snake River Plain, Idaho: American Journal of Science, v. 275, p. 225–251, doi: 10.2475/ajs.275.3.225.

Bartholomay, R.C., and Twining, B. V., 2015, Hydrologic Influences on Water-Level Changes in the Eastern Snake River Plain Aquifer at and near the Idaho National Laboratory , Idaho , 1949 – 2014 Scientific Investigations Report 2015 – 5085: U. S. Geological Survey Scientific Investigations Report, v. 2015-5085, p. 37.

Bestland, E.A., Link, P.K., Lanphere, M.A., and Champion, D.E., 2002, Paleoenvironments of sedimentary interbeds in the Pliocene and Quaternary Big Lost Trough (eastern Snake River Plain, Idaho): Geological Society of America Special Paper, v. 353, p. 27–44.

Bindeman, I.N., and Simakin, A.G., 2014, Rhyolites — Hard to produce , but easy to recycle and sequester : Integrating microgeochemical observations and numerical models: Geosphere, v. 10, no. 5, p. 930–957, doi: 10.1130/GES00969.1.

Bindeman, I.N., Watts, K.E., Schmitt, A.K., Morgan, L. a., and Shanks, P.W.C., 2007, Voluminous low δ18O magmas in the late Miocene Heise volcanic field, Idaho: Implications for the fate of Yellowstone hotspot calderas: Geology, v. 35, no. 11, p. 1019, doi: 10.1130/G24141A.1.

Bonnichsen, B., Leeman, W.P., Honjo, N., McIntosh, W.C., and Godchaux, M.M., 2007, Miocene silicic volcanism in southwestern Idaho: geochronology, geochemistry, and evolution of the central Snake River Plain: Bulletin of Volcanology, v. 70, p. 315–342, doi: 10.1007/s00445-007-0141-6.

Braile, L.W., Smith, R.B., Ansorge, J., Baker, M.R., Sparlin, M.A., Prodehl, C., Schilly, M.M., Healy, J.H., Mueller, S., and Olsen, K.H., 1982, The Yellowstone-Snake River Plain seismic profiling experiment: Crustal structure of the Eastern Snake River Plain: Journal of Geophyscial Research, v. 87, no. B4, p. 2597–2609.

Branney, M., and Acocella, V., 2015, Calderas, *in* Sigurdsson, J., Houghton, B., McNutt, S.R., and Stix, J. eds., Encyclopedia of volcanoes, Elsevier/Academic Press, New York.

Branney, M.J., Bonnichsen, B., Andrews, G.D.M., Ellis, B., Barry, T.L., and McCurry, M., 2008, "Snake River (SR)-type" volcanism at the Yellowstone hotspot track: Distinctive products from unusual, high-temperature silicic super-eruptions: Bulletin of Volcanology, v. 70, p. 293–314, doi: 10.1007/s00445-007-0140-7.

Brott, A., Blackwell, D.D., and Ziagos, J.P., 1981, Thermal and tectonic implications of heat flow in the Eastern Snake River Plain , Idaho: Journal of Geophyscial Research, v. 86, no. B12, p. 11709–11734.

Bruhn, R.L., Wu, D., and Lee, J.-J., 1992, Final report on structure of the southern Lemhi and Arco Fault Zone, Idaho. EGG-NPR-10680 Informal Report prepared for U.S. Department of Energy.

Camp, V.E., Pierce, K.L., and Morgan, L.A., 2015, Yellowstone plume trigger for Basin and Range extension, and coeval emplacement of the Nevada–Columbia Basin magmatic belt: Geosphere , v. 11 , no. 2 , p. 203–225, doi: 10.1130/GES01051.1.

Carpenter, N.S., and Payne, S.J., 2009, Deep, long-period earthquakes in and around Craters of the Moon National Monument, Idaho: Seismological Research Letters, v. 80, p. 350.

Champion, D.E., Hodges, M.K. V., Davis, L.C., and Lanphere, M.A., 2011, Paleomagnetic Correlation of Surface and Subsurface Basaltic Lava Flows and Flow Groups in the Southern Part of the Idaho National Laboratory , Idaho , with Pleomagnetic Data Tables for Drill Cores Scientific Investigations Report 2011 – 5a049: U. S. Geological Survey Scientific Investigations Report, v. 2011-5049, p. 33.

Champion, D.E., Lanphere, M.A., and Kuntz, M.A., 2002, Accumulation and subsidence of late Pleistocene basaltic lava flows of the eastern Snake River Plain, Idaho, *in* Link, P.K. and Mink, L.L. eds., Geological Society of America Special Paper, Geological Society of America, p. 175–192.

Christiansen, E.H., and McCurry, M., 2008, Contrasting origins of Cenozoic silicic volcanic rocks from the western Cordillera of the United States: Bulletin of Volcanology, v. 70, no. 3, p. 251–267, doi: 10.1007/s00445-007-0138-1.

Cole, J., Milner, D., and Spinks, K., 2005, Calderas and caldera structures: a review: Earth-Science Reviews, v. 69, no. 1-2, p. 1–26, doi: 10.1016/j.earscirev.2004.06.004.

DeCelles, P.G., and Coogan, J.C., 2006a, Regional structure and kinematic history of the Sevier fold-and-thrust belt, central Utah: Geological Society of America Bulletin, v. 118, no. 7-8, p. 841–864, doi: 10.1130/B25759.1.

DeNosaquo, K.R., Smith, R.B., and Lowry, A.R., 2009, Density and lithospheric strength models of the Yellowstone-Snake River Plain volcanic system from gravity and heat flow data: Journal of Volcanology and Geothermal Research, v. 188, no. 1-3, p. 108–127, doi: 10.1016/j.jvolgeores.2009.08.006.

de Silva, S.L., Mucek, A.E., Gregg, P.M., and Pratomo, I., 2015, Resurgent Toba - field, chronologic, and model constraints on time scales and mechanisms of resurgence at large calderas: Frontiers in Earth Science, v. 3, p. 1–17, doi: 10.3389/feart.2015.00025.

Dickinson, W.R., 2004, Evolution of the North American Cordillera: Annual Review of Earth and Planetary Sciences, v. 32, no. 1, p. 13–45, doi: 10.1146/annurev.earth.32.101802.120257.

Doherty, D.J., 1979b, Drilling data from exploration well 2-2A, NW1/4, Sec. 15, T. 5 N., R. 31 E., Idaho National Engineering Laboratory, Butte County, Idaho: U. S. Geological Survey Open-File Report, v. 79-851, p. 1.

Doherty, D., McBroome, L., and Kuntz, M., 1979, Preliminary geological interpretation and lithologic log of the exploratory geothermal test well (INEL-1): U. S. Geological Survey Open-File Report, v. 79-1248, p. 10.

Drew, D.L., Bindeman, I.N., Watts, K.E., Schmitt, A.K., Fu, B., and McCurry, M., 2013, Crustal-scale recycling in caldera complexes and rift zones along the Yellowstone hotspot track: O and Hf isotopic evidence in diverse zircons from voluminous rhyolites of the Picabo volcanic field, Idaho: Earth and Planetary Science Letters, v. 381, p. 63–77, doi: 10.1016/j.epsl.2013.08.007.

Ekren, E.B., McIntyre, D.H., and Bennett, E.H., 1984, High-temperature, large-volume, lavalike ash-flow tuffs without caldera in southwestern Idaho: U.S. Geological Survey Proffesional Paper, v. 1272, p. 82.

Ellis, B.S., Wolff, J. a., Boroughs, S., Mark, D.F., Starkel, W. a., and Bonnichsen, B., 2013, Rhyolitic volcanism of the central Snake River Plain: a review: Bulletin of Volcanology, v. 75, no. 8, p. 745, doi: 10.1007/s00445-013-0745-y.

Embree, G.F., Lowell, M.D., and Doherty, D.J., 1978, Drilling data from Sugar City exploration well, Madison County, Idaho: U. S. Geological Survey Open-File Report, v. 78-1095, p. 1.

Fishel, M.L., 1993, The geology of uplifted rocks on Big Southern Butte: implications for the stratigraphy and geochemistry of the eastern Snake River plain, Idaho: Idaho State University, 178 p.

Foster, D.A., Mueller, P.A., Mogk, D.W., Wooden, J.L., and Vogl, J.J., 2006, Proterozoic evolution of the western margin of the Wyoming craton: implications for the tectonic and magmatic evolution of the northern Rocky Mountains: Canadian Journal of Earth Sciences, v. 43, no. 10, p. 1601–1619, doi: 10.1139/e06-052.

Fouch, M.J., 2012, The Yellowstone Hotspot : Plume or Not ? Geology, , no. 5, p. 479–480, doi: 10.1016/j.

Foulger, G.R., Christiansen, R.L., and Anderson, D.L., 2015, The Yellowstone “hot spot” track results from migrating basin-range extension: Geological Society of America Special Paper, v. 514, p. SPE514–14, doi: 10.1130/2015.2514(14).

Gaschnig, R.M., Vervoort, J.D., Lewis, R.S., and Tikoff, B., 2011, Isotopic Evolution of the Idaho Batholith and Challis Intrusive Province, Northern US Cordillera: Journal of Petrology, v. 52, no. 12, p. 2397–2429, doi: 10.1093/petrology/egr050.

Geslin, J.K., Link, P.K., Riesterer, J.W., Kuntz, M.A., and Fanning, C.M., 2002, Pliocene and Quaternary stratigraphic architecture and drainage systems of the Big Lost Trough, northeastern Snake River Plain, Idaho: Geological Society of America Special Paper, v. 353, p. 11–26.

Geyer, A., and Martí, J., 2008, The new worldwide collapse caldera database (CCDB): A tool for studying and understanding caldera processes: Journal of Volcanology and Geothermal Research, v. 175, no. 3, p. 334–354, doi: 10.1016/j.jvolgeores.2008.03.017.

Greely, R., and King, J.S., 1977, Volcanism of the Eastern Snake River Plain, Idaho: A comparative planetary geology guidebook (R. Greely & J. S. King, Eds.): NASA, Washington, D.C.

Greensfelder, R.W., and Kovach, R.L., 1982, Shear wave velocities and crustal structure of the Eastern Snake River Plain, Idaho: Journal of Geophyscial Research, v. 87, no. B4, p. 2643–2653.

Gregg, P.M., De Silva, S.L., Grosfils, E.B., and Parmigiani, J.P., 2012, Catastrophic caldera-forming eruptions: Thermomechanics and implications for eruption triggering and maximum caldera dimensions on Earth: Journal of Volcanology and Geothermal Research, v. 241-242, p. 1–12, doi: 10.1016/j.jvolgeores.2012.06.009.

Hackett, W.R., and Smith, R.P., 1992, Quaternary volcanism, tectonics, and sedimentation in the Idaho National Engineering Laboratory area, *in* Wilson, J.R. ed., Field Guide to Geological Excursions in Utah and Adjacent Areas of Nevada, Idaho, and Wyoming, Utah Geological Survey Miscellaneous Publication 92-3, p. 1–18.

Holmes, A. a. J., Rodgers, D.W., and Hughes, S.S., 2008, Kinematic analysis of fractures in the Great Rift, Idaho: Implications for subsurface dike geometry, crustal extension, and magma dynamics: Journal of Geophysical Research, v. 113, no. B4, p. 1–15, doi: 10.1029/2006JB004782.

Hughes, S.S., Wetmore, P.H., and Casper, J.L., 2002, Evolution of Quaternary Tholeiitic Basalt Eruptive Centers on the Eastern Snake River Plain , Idaho, *in* Tectonic and Magmatic Evolution of the Snake River Plain Volcanic Province,.

Jackson, S.M., Carpenter, G.S., Smith, R.P., and Casper, J.L., 2006, Seismic reflection project near the southern terminations of the Lost River and Lemhi Faults , Eastern Snake River Plain , Idaho: Idaho National Laboratory Report, v. INL/EXT-06, no. October, p. 16.

Janecke, S.U., 1993a, Structures in segment boundary zones of the Lost River and Lemhi Faults, east central Idaho: Journal of Geophysical Research, v. 98, no. B9, p. 16,223–16,238.

Josten, N.E., and Smith, R.P., 1997, Gravity evidence for buried calderas beneath the eastern Snake River Plain: Geological Society of America Abstacts, v. 29, p. 365.

Kawakami, Y., Hoshi, H., and Yamaguchi, Y., 2007, Mechanism of caldera collapse and resurgence: Observations from the northern part of the Kumano Acidic Rocks, Kii peninsula, southwest Japan: Journal of Volcanology and Geothermal Research, v. 167, no. 1-4, p. 263–281, doi: 10.1016/j.jvolgeores.2007.02.003.

Kelbert, a., Egbert, G.D., and deGroot-Hedlin, C., 2012, Crust and upper mantle electrical conductivity beneath the Yellowstone Hotspot Track: Geology, v. 40, no. 5, p. 447–450, doi: 10.1130/G32655.1.

Kellogg, K.S., Harlan, S.S., Mehnert, H.H., Snee, L.W., Pierce, K.L., Hackett, W.R., and Rodgers, D.W., 1994, Major 10 . 2-Ma Rhyolitic Volcanism in the Eastern Snake River Plain , Idaho- Isotopic Age and Stratigraphic Setting of the Arbon Valley Tuff Member of the Starlight Formation. U. S. Geological Survey Bulletin, v. 2091, p. 18.

Kennedy, B., Wilcock, J., and Stix, J., 2012, Caldera resurgence during magma replenishment and rejuvenation at Valles and Lake City calderas: Bulletin of Volcanology, v. 74, no. 8, p. 1833–1847, doi: 10.1007/s00445-012-0641-x.

Knott, T., Branney, M.J., Christiansen, E.H., Reichow, M.K., McCurry, M.O., and Shervais, J.W., 2013, Drilling a “;super-volcano”: volcanology of the proximal rhyolitic volcanic succession in the HOTSPOT deep drill hole, Idaho, Yellowstone hot-spot track: American Geophysical Union Abstract V13D-2649.

Konstantinou, A., and Strickland, A., 2012, Multistage Cenozoic extension of the Albion–Raft River–Grouse Creek metamorphic core complex: Geochronologic and stratigraphic constraints: Geosphere, v. 8, no. 6, p. 1429–1466.

Konstantinou, A., Valley, J.W., Strickland, A., Miller, E.L., Fisher, C., Vervoort, J., and Wooden, J.L., 2013, Geochemistry and geochronology of the Jim Sage volcanic suite, southern Idaho: Implications for Snake River Plain magmatism and its role in the history of Basin and Range extension: Geosphere, v. 9, no. 6, p. 1681–1703, doi: 10.1130/GES00948.1.

Konstantinou, A., Strickland, A., Miller, E., Vervoort, J., Fisher, C.M., Wooden, J., and Valley, J., 2013, Synextensional magmatism leading to crustal fl ow in the Albion – Raft River – Grouse Creek metamorphic core complex , northeastern Basin and Range: Tectonics, v. 32, p. 1–20, doi: 10.1002/tect.20085.

Kuntz, M.A., 1992, A model-based perspective of basaltic volcanism, eastern Snake River Plain, Idaho, *in* Link, P.K., Kuntz, M.A., and Platt, L.B. eds., Regional Geology of Eastern Idaho and Western Wyoming, Geological Society of America Memoir 179, p. 289–304.

Kuntz, M.A., Anderson, S.R., Champion, D.E., Lanphere, M.A., and Grunwald, D.J., 2002, Tension cracks, eruptive fissures, dikes, and faults related to late Pleistocene-Holocene basaltic volcanism and implications for the distribution of hydraulic conductivity in the eastern Snake River Plain, Idaho: Geological Society of America Special Paper, v. 353, p. 111–133.

Kuntz, M. a., Champion, D.E., Spiker, E.C., and Lefebvre, R.H., 1986b, Contrasting magma types and steady-state, volume-predictable, basaltic volcanism along the Great Rift, Idaho (USA).: Geological Society of America Bulletin, v. 97, no. 5, p. 579–594.

Kuntz, M.A., Covington, H.R., and Schorr, L.J., 1992, An overview of basaltic volcanism of the eastern Snake River Plain, Idaho, *in* Link, P.K., Kuntz, M.A., and Platt, L.B. eds., Geological Society of America Memoir, Geological Society of America, p. 227–267.

Kuntz, M.A., and Dalrymple, G.B., 1979, Geology, geochronology, and potential volcanic hazards in the Lava Ridge-Hells Half Acre area, eastern Snake River Plain, Idaho: U. S. Geological Survey Open-File Report, v. 79-1657, p. 66.

Kuntz, M.A., and Kork, J.O., 1978, Geology of the Arco-Big Southern Butte area, eastern Snake RiverPlain, and potential volcanic hazards to the radioactive waste management complex, and other waste storage and reactor facilities at the Idaho National Engineering Laboratory, Idaho: U. S. Geological Survey Open-File Report, v. 78-691, p. 77.

Kuntz, M.A., Skipp, B.A., Lanphere, M.A., Scott, W.E., Pierce, K.L., Dalrymple, G. B. Champion, D.E., Embree, G.F., Page, W.R., Morgan, L.A., Smith, R.P., Hackett, W.R., and Rodgers, D.W., 1994, Geologic map of the Idaho National Engineering Laboratory and adjoining areas, eastern Idaho: U. S. Geological Survey IMAP, v. 2330.

Leeman, W.P., Annen, C., and Dufek, J., 2008, Snake River Plain - Yellowstone silicic volcanism: implications for magma genesis and magma fluxes: Geological Society, London, Special Publications, v. 304, no. 1, p. 235–259, doi: 10.1144/SP304.12.

Leeman, W.P., Schutt, D.L., and Hughes, S.S., 2009, Thermal structure beneath the Snake River Plain: Implications for the Yellowstone hotspot: Journal of Volcanology and Geothermal Research, v. 188, no. 1-3, p. 57–67, doi: 10.1016/j.jvolgeores.2009.01.034.

Leeman, W.P., 1982, Evolved and Hybrid Lavas from the Snake River Plain, Idaho, *in* Bonnichsen, B. and Breckenridge, R.M. eds., Cenozoic Geology of Idaho, Idaho Bureau of Mines and Geology Bulletin 26, p. 193–202.

Liberty, L.M., Schmitt, D.R., and Shervais, J.W., 2015, Seismic imaging through the volcanic rocks of the Snake River Plain: insights from Project Hotspot: Geophysical Prospecting, v. 63, p. 919–936, doi: 10.1111/1365-2478.12277.

Link, P.K., and Janecke, S.U., 1999, Geology of East-Central Idaho: Geologic Roadlogs for the Big and Little Lost River, Lemhi, and Salmon River Valleys, *in* Hughes, S.S. and Thackray, G.D. eds., Guidebook to the Geology of Eastern Idaho, Idaho Museum of Natural History, p. 295–334.

Lipman, P.W., Zimmerer, M.J., and McIntosh, W.C., 2015, An ignimbrite caldera from the bottom up: Exhumed floor and fill of the resurgent Bonanza caldera, Southern Rocky Mountain volcanic field, Colorado: Geosphere, v. 11, p. GES01184.1, doi: 10.1130/GES01184.1.

Lipman, P.W., and McIntosh, W.C., 2008, Eruptive and noneruptive calderas, northeastern San Juan Mountains, Colorado: Where did the ignimbrites come from? Bulletin of the Geological Society of America, v. 120, p. 771–795, doi: 10.1130/B26330.1.

Lipman, P.W., 1997, Subsidence of ash-flow calderas: relation to caldera size and magma-chamber geometry: Bulletin of Volcanology, v. 59, no. 3, p. 198–218, doi: 10.1007/s004450050186.

Mabey, D.R., 1982, Geophysics and tectonics of the Snake River plain, Idaho: Bulletin - Idaho Bureau of Mines and Geology, v. 26, p. 139.

Mabey, D.R., 1978, Gravity and aeromagnetic anomalies in the Rexburg area of Eastern Idaho: U. S. Geological Survey Open-File Report, v. 78-382, p. 19.

McCurry, M., 2009, The Arbon Valley Tuff: A new look at a highly anomalous ignimbrite from the Yellowstone–Snake River Plain track: Geological Society of America Abstracts with Programs, v. 41, no. 6, p. 43.

McCurry, M., Hayden, K.P., Morse, L.H., and Mertzman, S., 2008, Genesis of post-hotspot, A-type rhyolite of the Eastern Snake River Plain volcanic field by extreme fractional crystallization of olivine tholeiite: Bulletin of Volcanology, v. 70, no. 3, p. 361–383, doi: 10.1007/s00445-007-0143-4.

McCurry, M., and Rodgers, D.W., 2009, Mass transfer along the Yellowstone hotspot track I: Petrologic constraints on the volume of mantle-derived magma: Journal of Volcanology and Geothermal Research, v. 188, no. 1-3, p. 86–98, doi: 10.1016/j.jvolgeores.2009.04.001.

McCurry, M., and Welhan, J., 2012, Do Magmatic-Related Geothermal Energy Resources Exist in Southeast Idaho ? GRC Transactions, v. 36, p. 699–707.

McBroome, L.A., Doherty, D.J., and Embree, G.F., 1981, Correlation of major Pliocene and Miocene ash-flow sheets, eastern Snake River plain, Idaho, *in* Montana Geological Society 1981 Field Conference and Symposium Guidebook to Southwest Montana, p. 323–330.

McQuarrie, N., and Rodgers, D.W., 1998, Subsidence of a volcanic basin by flexure and lower crustal flow: The eastern Snake River Plain, Idaho: Tectonics, v. 17, no. 2, p. 203, doi: 10.1029/97TC03762.

Moody, A., and Plummer, M. a, 2014, Implications of geology, structure and tectonic setting for heat extraction on the Eastern Snake River Plain: Proceedings, Thirty-Ninth Workshop on Geothermal Reservoir Engineering Stanford University, Stanford, California, February 24-26, 2014 SGP-TR-202, v. 2, no. SGP-TR-202, p. 1–9.

Morgan, L.A., 1988, Explosive rhyolitic volcanism on the Eastern Snake River Plain: University of Hawaii, 200 p.

Morgan, L.A., 1992, Stratigraphic relations and paleomagnetic and geochemical correlations of ignimbrites of the Heise volcanic field, eastern Snake River Plain, eastern Idaho and western Wyoming, *in* Link, P.K., Kuntz, M.A., and Platt, L.B. eds., Geological Society of America Memoir, Geological Society of America, p. 215–226.

Morgan, L. a., Doherty, D.J., and Leeman, W.P., 1984, Ignimbrites of the Eastern Snake River Plain: Evidence for major caldera-forming eruptions: Journal of Geophysical Research, v. 89, no. B10, p. 8665, doi: 10.1029/JB089iB10p08665.

Morgan, L. a., and McIntosh, W.C., 2005, Timing and development of the Heise volcanic field, Snake River Plain, Idaho, western USA: Geological Society of America Bulletin, v. 117, no. 3, p. 288, doi: 10.1130/B25519.1.

Morgan, L.A., Pierce, K.L., and Shanks, W.C.P., 2008, Track of the Yellowstone hotspot: Young and ongoing geologic processes from the Snake River Plain to the Yellowstone Plateau and Tetons, *in* Roaming the Rocky Mountains and Environs: Geological Field Trips: Geological Society of America Field Guide, p. 1–35.

Pankratz, L.W., and Ackermann, H.D., 1982, Structure along the northwest edge of the Snake River Plain interpreted from seismic refraction: Journal of Geophysical Research, v. 87, no. B4, p. 2676, doi: 10.1029/JB087iB04p02676.

Parsons, T., 1995, The Basin and Range Province, *in* K. Olsen ed., Continental Rifts: Evolution, Structure and Tectonics, Elsevier, New York, p. 277– 324,.

Parsons, T., Thompson, G.A., and Smith, R.P., 1998a, More than one way to stretch: a tectonic model for extension along the plume track of the Yellowstone hotspot and adjacent Basin and Range Province: Tectonics, v. 17, no. 2, p. 221, doi: 10.1029/98TC00463.

Payne, S.J., McCaffrey, R., King, R.W., and Kattenhorn, S. a., 2012, A new interpretation of deformation rates in the Snake River Plain and adjacent basin and range regions based on GPS measurements: Geophysical Journal International, v. 189, no. 1, p. 101–122, doi: 10.1111/j.1365-246X.2012.05370.x.

Peng, X., and Humphreys, E.D., 1998, Crustal velocity structure across the eastern Snake River Plain and the Yellowstone swell: Journal of Geophyscial Research, v. 103, p. 7171–7186.

Phillips, W.M., Szymanowski, D., and Ellis, B., 2014, Effect of poorly constrained caldera locations on ignimbrite volume estimates, Heise Volcanic Field, Eastern Snake River Plain, Idaho: Geological Society of America Abstracts with Programs, v. 46, no. 5, p. 94.

Pierce, K.L., and Morgan, L. a., 2009, Is the track of the Yellowstone hotspot driven by a deep mantle plume? — Review of volcanism, faulting, and uplift in light of new data: Journal of Volcanology and Geothermal Research, v. 188, no. 1-3, p. 1–25, doi: 10.1016/j.jvolgeores.2009.07.009.

Pierce, K.L., and Morgan, L.A. The track of the Yellowstone hot s1oot: Volcanism, faulting, and uplift: Geological Society of America Memoir, v. 179, p. 1–52.

Podgorney, R., Mccurry, M., Wood, T., Mcling, T., Ghassemi, A., Welhan, J., Mines, G., Plummer, M., Moore, J., Fairley, J., and Wood, R., 2013, Enhanced Geothermal System Potential for Sites on the Eastern Snake River Plain , Idaho: GRC Transactions, v. 37, p. 191–197.

Potter, K.E., 2014, The Kimama Core: A 6.4 Ma record of volcanism , sedimentation , and magma petrogenesis on the axial volcanic high , Snake River Plain , ID: Utah State University PhD Dissertation, 174 p.

Putirka, K.D., Kuntz, M. a., Unruh, D.M., and Vaid, N., 2009, Magma Evolution and Ascent at the Craters of the Moon and Neighboring Volcanic Fields, Southern Idaho, USA: Implications for the Evolution of Polygenetic and Monogenetic Volcanic Fields: Journal of Petrology, v. 50, no. 9, p. 1639–1665, doi: 10.1093/petrology/egp045.

Rodgers, D.W., Hackett, W.R., and Ore, H.T., 1990, Extension of the Yellowstone plateau, eastern Snake River Plain, and Owyhee plateau: v. Geology, no. 18, p. 1138–1141.

Rodgers, D.W., Ore, H.T., and Bobo, R.T., 2002, Extension and subsidence of the eastern Snake River Plain, Idaho: Tectonic and Magmatic Evoluiton of the Snake River Plain Volcanic Province, p. 121–155.

Schmandt, B., Dueker, K., Humphreys, E., and Hansen, S., 2012, Hot mantle upwelling across the 660 beneath Yellowstone: Earth and Planetary Science Letters, v. 331-332, p. 224–236, doi: 10.1016/j.epsl.2012.03.025.

Shervais, J.W., Schmitt, D.R., Nielson, D., Evans, J.P., Christiansen, E.H., Morgan, L., Pat Shanks, W.C., Prokopenko, A. a., Lachmar, T., Liberty, L.M., Blackwell, D.D., Glen, J.M., Champion, D., Potter, K.E., et al., 2013, First results from HOTSPOT: The Snake River plain scientific drilling project, Idaho, U.S.A.: Scientific Drilling, , no. 15, p. 36–45, doi: 10.2204/iodp.sd.15.06.2013.

Shervais, J.W., Vetter, S.K., and Hanan, B.B., 2006, Layered mafic sill complex beneath the eastern Snake River Plain: Evidence from cyclic geochemical variations in basalt: Geology, v. 34, no. 5, p. 365–368, doi: 10.1130/G22226.1.

Skipp, B., Snider, L.G., Janecke, S.U., and Kuntz, M. A, 2009, Geologic map of the Arco 30 x 60 minute quadrangle, Idaho: Idaho Geologic Survey Publication GM-47. doi: 10.1029/2003GC000661.

Smith, R.B., Jordan, M., Steinberger, B., Puskas, C.M., Farrell, J., Waite, G.P., Husen, S., Chang, W.-L., and O'Connell, R., 2009, Geodynamics of the Yellowstone hotspot and mantle plume: Seismic and GPS imaging, kinematics, and mantle flow: Journal of Volcanology and Geothermal Research, v. 188, no. 1-3, p. 26–56, doi: 10.1016/j.jvolgeores.2009.08.020.

Smith, R.B., and Braile, L.W., 1994, The Yellowstone hotspot: Journal of Volcanology and Geothermal Research, v. 61, p. 121–187.

Smith, R.L., and Bailey, R.A., 1968, Resurgent cauldrons: Geological Society of America Memoir, p. 613–662, doi: 10.1130/MEM116-p613.

Sparlin, M.A., and Braile, L.W., 1982, Crustal structure of the Eastern Snake River Plain determined from ray trace modeling of seismic refraction data: Journal of Geophyscial Research, v. 87, no. B4, p. 2619–2633.

Spear, D.B., and King, J.S., 1982, The geology of Big Southern Butte, Idaho, *in* Cenozoic Geology of Idaho, Idaho Bureau of Mines and Geology Bulletin 26, p. 395–403.

Spera, F.J., and Crisp, J.A., 1981, Eruption volume, periodicity, and caldera area: Relationships and inferences on development of compositional zonation in silicic magma chambers: Journal of Volcanology and Geothermal Research, v. 11, p. 169–187.

Strickland, a., Miller, E.L., Wooden, J.L., Kozdon, R., and Valley, J.W., 2011, Syn-extensional plutonism and peak metamorphism in the Albion-Raft River-Grouse Creek metamorphic core complex: American Journal of Science, v. 311, no. 4, p. 261–314, doi: 10.2475/04.2011.01.

Strickland, A., Miller, E.L., and Wooden, J.L., 2011, The Timing of Tertiary Metamorphism and Deformation in the Albion–Raft River–Grouse Creek Metamorphic Core Complex, Utah and Idaho: The Journal of Geology, v. 119, no. 2, p. 185–206, doi: 10.1086/658294.

Szymanowski, D., Ellis, B.S., Bachmann, O., Guillong, M., and Phillips, W.M., 2015, Bridging basalts and rhyolites in the Yellowstone–Snake River Plain volcanic province: The elusive intermediate step: Earth and Planetary Science Letters, v. 415, p. 80–89, doi: 10.1016/j.epsl.2015.01.041.

Vogl, J.J., Min, K., Carmenate, a., Foster, D. a., and Marsellos, a., 2014, Miocene regional hotspot-related uplift, exhumation, and extension north of the Snake River Plain: Evidence from apatite (U-Th)/He thermochronology: Lithosphere, v. 6, no. 2, p. 108–123, doi: 10.1130/L308.1.

Wagner, L.S., Fouch, M.J., James, D.E., and Hanson-Hedgecock, S., 2012, Crust and upper mantle structure beneath the Pacific Northwest from joint inversions of ambient noise and earthquake data: Geochemistry, Geophysics, Geosystems, v. 13, no. 12, p. n/a–n/a, doi: 10.1029/2012GC004353.

Walker, G.P.L., 1984, Downsag calderas, ring faults, caldera sizes, and incremental caldera growth: Journal of Geophysical Research, v. 89, no. B10, p. 8407–8416, doi: 10.1029/JB089iB10p08407.

Watts, K.E., Bindeman, I.N., and Schmitt, A.K., 2011, Large-volume rhyolite genesis in caldera complexes of the Snake River Plain: Insights from the Kilgore Tuff of the Heise volcanic field, Idaho, with comparison to Yellowstone and Bruneau-Jarbidge rhyolites: Journal of Petrology, v. 52, no. 5, p. 857–890, doi: 10.1093/petrology/egr005.

Wetmore, P.H., Hughes, S.S., Connor, L., and Caplinger, M., 2009, Spatial distribution of eruptive centers about the Idaho National Laboratory, *in* Connor, C.B., Chapman, N.A., and Connor, L.J. eds., Volcanic and Tectonic Assessment for Nuclear Facilities, Cambridge, UK, Cambridge University Press, p. 23.

Whitaker, M.L., Nekvasil, H., Lindsley, D.H., and McCurry, M., 2008, Can crystallization of olivine tholeiite give rise to potassic rhyolites? - An experimental investigation: Bulletin of Volcanology, v. 70, p. 417–434, doi: 10.1007/s00445-007-0146-1.

Willcock, M. a W., Cas, R. a F., Giordano, G., and Morelli, C., 2013, The eruption, pyroclastic flow behaviour, and caldera in-filling processes of the extremely large volume (>1290km3), intra- to extra-caldera, Permian Ora (Ignimbrite) Formation, Southern Alps, Italy: Journal of Volcanology and Geothermal Research, v. 265, p. 102–126, doi: 10.1016/j.jvolgeores.2013.08.012.

Wohletz, K., and Heiken, G., 1992, Volcanology and geothermal energy: University of California Press, Berkeley, California.

Wu, D., and Bruhn, R.L., 1994, Structural and rupture characteristics of the southern Lost River Fault Zone, Idaho:.

Yonkee, W. a., Dehler, C.D., Link, P.K., Balgord, E. a., Keeley, J. a., Hayes, D.S., Wells, M.L., Fanning, C.M., and Johnston, S.M., 2014, Tectono-stratigraphic framework of Neoproterozoic to Cambrian strata, west-central U.S.: Protracted rifting, glaciation, and evolution of the North American Cordilleran margin: Earth-Science Reviews, v. 136, p. 59–95, doi: 10.1016/j.earscirev.2014.05.004.

Yuan, H., Dueker, K., and Stachnik, J., 2010, Crustal structure and thickness along the Yellowstone hot spot track: Evidence for lower crustal outflow from beneath the eastern Snake River Plain: Geochemistry, Geophysics, Geosystems, v. 11, no. 3, doi: 10.1029/2009GC002787.

Zhdanov, M.S., Gribenko, A., Čuma, M., and Green, M., 2012, Geoelectrical Structure of the Lithosphere and Asthenosphere beneath the Northwestern United States: Geology & Geosciences, v. 1, no. 2, p. 1–6, doi: 10.4172/jgg.1000106.

Zhdanov, M.S., Smith, R.B., Gribenko, A., Cuma, M., and Green, M., 2011, Three-dimensional inversion of large-scale EarthScope magnetotelluric data based on the integral equation method: Geoelectrical imaging of the Yellowstone conductive mantle plume: Geophysical Research Letters, v. 38, no. 8, p. n/a–n/a, doi: 10.1029/2011GL046953.

Zohdy, A.A.R., and Stanley, W.D., 1973, Preliminary interpretation of electrical sounding curves obtained across the Snake River Plain from Blackfoot to Arco, Idaho: U. S. Geological Survey Open-File Report, v. 73-370.